Liu *et al. Chem Synth* 2022;2:7
DOI: 10.20517/cs.2022.01

Chemical Synthesis

Review

Open Access

Check for updates

Recent advances in circularly polarized luminescence generated by inorganic materials

Xinling Liu[1], Ren-Hua Jin[2,*]

[1]The Education Ministry Key Lab of Resource Chemistry, College of Chemistry and Materials Science, Shanghai Normal University, Shanghai 200234, China.
[2]Department of Material and Life Chemistry, Kanagawa University, Yokohama 221-8686, Japan.

Correspondence to: Prof. Ren-Hua Jin, Department of Material and Life Chemistry, Kanagawa University, 3-27-1 Rokkakubashi, Kanagawa-ku, Yokohama-shi, Yokohama 221-8686, Japan. E-mail: rhjin@kanagawa-u.ac.jp

How to cite this article: Liu X, Jin RH. Recent advances in circularly polarized luminescence generated by inorganic materials. *Chem Synth* 2022;2:7. https://dx.doi.org/10.20517/cs.2022.01

Received: 5 Jan 2022 **First Decision:** 7 Feb 2022 **Revised:** 23 Feb 2022 **Accepted:** 24 Feb 2022 **Published:** 24 Feb 2022

Academic Editor: Bao-Lian Su **Copy Editor:** Jia-Xin Zhang **Production Editor:** Jia-Xin Zhang

Abstract

Circularly polarized luminescence (CPL) is an interesting phenomenon that represents the unequal emission of left- and right-handed polarized light from an emitter. CPL is promising in chirality characterization and various optical applications. Traditionally, research on CPL has been centered on organic substances. Nevertheless, in recent years, CPL based on inorganic substrates has also become a nascent topic, which is significant in exploring novel chirality- and luminescence-related properties and applications in inorganic materials. This short review summarizes the recent progress made regarding the following two aspects: 1) how to endow common inorganic luminophores with CPL activity; 2) how to use emerging chiral inorganic nanomaterials to design CPL-active systems. The general synthesis strategies, optical properties, applications and outlook of CPL-active inorganic materials are also demonstrated.

Keywords: Circularly polarized luminescence, chirality, luminescence, inorganic luminescent materials, inorganic chiral materials

INTRODUCTION

Chirality is termed as the phenomenon where a certain object is nonsuperposable on its mirror image. When two objects with such a relationship exist, they are known as enantiomers. Chirality is pervasive and manifests itself at different scales, ranging from macroscopic left and right hands to molecular-scale

asymmetric carbon atoms and to various helical structures [Figure 1A-C]. The significance of chirality is well acknowledged, for example, only one given enantiomeric form of many biomolecules is preferred to maintain life. The above homochirality of life also raises an exacting enantiomer selectivity toward numerous daily chemicals, drugs and pesticides. Therefore, understanding chiral structure-property relationships is one of the most important topics across a broad range of disciplines[1,2].

Light can also be chiral in the form of circularly polarized (CP) light. As shown in Figure 1D, around the direction of propagation, the electric field of CP light rotates in either a counterclockwise or clockwise helical pattern, resulting in left-handed CP light (LCP) or its counter-enantiomer of right-handed CP light (RCP), respectively. CP light has many promising applications, including three-dimensional (3D) and holographic display, spintronics, encryption, diagnosis and asymmetric synthesis[3-10]. Traditionally, a combination of a linear polarizer and a quarter-wave plate is applied to obtain CP light. However, this method suffers from a severe loss of light, especially in LED displays (up to 50%), invalidity beyond a certain frequency range and incompatibility with highly integrated photonic circuits[11,12]. Therefore, it is of interest to explore high-efficiency methods for the generation of CP light.

Usually, enantiomers are indistinguishable to some extent, since they share many identical properties. Fortunately, they respond differently toward LCP and RCP, which enables us to "see" microscale chiral matter using CP light-based spectroscopy[13,14]. Furthermore, the capability of chiral substances to manipulate the polarization states of light provides an alternative method to enable a luminophore to emit LCP and RCP beams unequally, which is known as circularly polarized luminescence (CPL)[15]. A schematic description for CPL in chiral systems is shown in Figure 1E. In principle, a pair of CPL-active enantiomers exhibit the same photoluminescence (PL) spectra. However, the LCP and RCP components in the emission are unequal when chirality is taken into consideration, *i.e.*, LCP is over than RCP in one enantiomer, while the reverse is true in the other enantiomer. By measuring the difference between LCP and RCP (denoted by "I_L-I_R", where I_L and I_R are the intensity of LCP and RCP, respectively) at a given emission wavelength, a CPL spectrum can be drawn using "I_L-I_R" as the vertical axis and emission wavelength as the horizontal axis. It is noted that the value of "I_L-I_R" is expressed as an ellipse angle θ (mdeg) in many studies and some commercial CPL instruments. This is because the overall polarization trajectory for a mixture of LCP and RCP light becomes an ellipse when I_L is unequal to I_R. The CPL signals usually overlap with the corresponding PL signals, but a pair of enantiomers show opposing CPL spectra.

Another important index to evaluate CPL is the dissymmetry factor of g_{lum}:g_{lum} = $[2(I_L-I_R)]/(I_L+I_R)$. For the values of g_{lum} ranging from -2 to +2, only a given handedness CP light is emitted in the extreme cases (+2 for LCP only and -2 for RCP only), while no circular polarization occurs (i.e., I_L=I_R) when g_{lum} is zero. Consequently, CPL spectroscopy affords a unique tool to study the chiral structures and properties of matter in excited states, is the emission analog of common circular dichroism (CD) spectroscopy and is supplementary to fluorescence spectroscopy. In return, the construction of various CPL-active chiral luminescent materials further expands the applications of CP light.

Over the past decade, notable progress has been made in the exploration of novel CPL-active systems, together with the advancement of CPL spectroscopy. However, much research has focused on organic substances, partially due to the fact that research on chirality has a long history in organic chemistry[16-21]. According to the principles of CPL in chiral systems, the choices of either luminescent or chiral unity should be diverse, thus allowing for a broad range of potential CPL-active systems beyond organics. On this basis, it is noteworthy that inorganic-based CPL has become a new and active research topic in recent years. For example, many inorganic luminophores are employed to create more colorful CPL candidates and

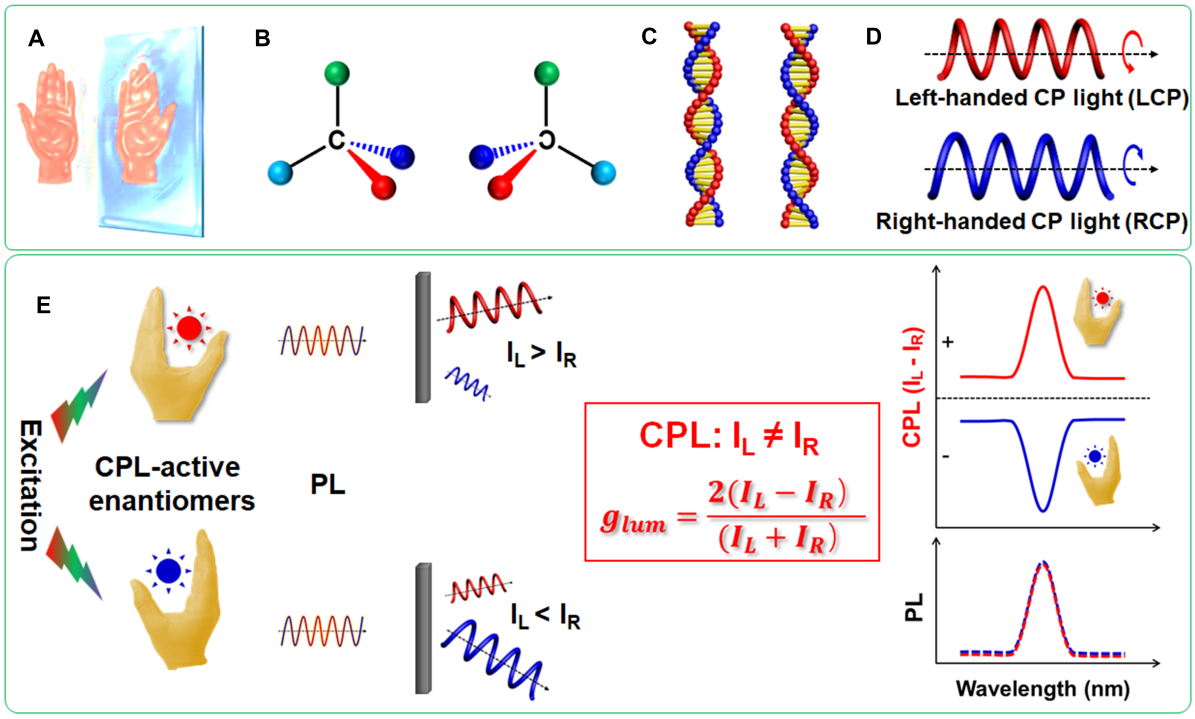

Figure 1. Typical enantiomers of (A) left and right hands, (B) chiral carbon centers, (C) helices and (D) left- and right-handed CP light. (E) Schematic of CPL from two CPL-active enantiomers. CPL: Circularly polarized luminescence.

emerging chiral inorganic nanomaterials are able to impart various luminophores with CPL activity[22,23]. Such research is significant for many reasons, including the fact that it brings a new perspective to explore the luminescence properties and mechanisms of inorganic luminophores, especially in chiral environments. In addition, it provides a toolbox to analyze the structures of chiral inorganic materials and is helpful in understanding the chirality transfer in "matter-matter" or "light-matter" interactions. Finally, it also offers more inorganic/organic functional materials with the power to manipulate light to broaden CPL-based applications[24-28].

In this short review, we consider two inorganic-associated CPL-active systems, namely, inorganic luminophore-containing and chiral inorganic host-based systems. For the former systems, various classes of inorganic luminophores are described, including metal ions (e.g., lanthanide and chromium ions), perovskite nanocrystals (NCs), metal clusters, carbon dots and semiconductors nanoparticles (NPs). Given that there are some recent well-written reviews focusing on lanthanide complexes, chromium complexes and perovskite NCs, they are discussed at length here. With regards to the latter systems, the utilization of chiral silica (SiO_2) nanomaterials, chiral inorganic crystals and helical inorganic assemblies as hosts for CPL is discussed. To demonstrate the recent progress in these systems, some typical examples are selected and discussed. The properties (components, construction strategies and excitation and emission wavelengths, g_{lum}) of these examples are summarized in Table 1.

We provide an overview of inorganic-based CPL. Firstly, several types of construction strategies for CPL-active systems are summarized, which are further clarified by selected examples of CPL-active systems containing inorganic luminophores or chiral inorganic nanomaterials. Next, CPL-active systems based on some special luminescent processes are listed, which are different from the common down-conversion

Table 1. Components, construction strategies and CPL properties of some inorganic-based CPL-active systems

Luminophore	Construction strategy type [chiral sources]	Excitation wavelength (nm)	Emission wavelength (nm)	Quantum yield (%)	Magnitude of g_{lum}
1. Inorganic luminophore-based CPL					
Yb^{3+}	II [PrPyBox, PhPyBOx]	365	972	0.60-0.70	10^{-2}, Ref.[78]
$NaYF_4$:Yb/Tm, $NaYF_4$:Yb/Er	III [L-/D-GAm assemblies]	980	360, 476, 802 (Tm), 540, 654 (Er)	N	10^{-3}, Ref.[88]
$CaAl_2O_4$:Eu, Nd	II [L-/D-cysteine]	320	440	N	10^{-2}, Ref.[81]
ZnO	I [L/D-methionine]	325	510	N	N , Ref.[36]
CdSe	II [L-/D-cysteine]	451	605	N	10^{-3}, Ref.[41]
CdSe/CdS	II [L-/D-cysteine]	400	583-683	35-60	10^{-4}, Ref.[64]
Ag clusters	I [see Figure 6A]	365	558	3.9	10^{-1}, Ref.[57]
Au clusters	I [see Figure 12A]	365	500	36.7	10^{-3}, Ref.[86]
Ag clusters	I [see Figure 12A]	N	574	56, 95	10^{-3}, Ref.[80]
AuAg clusters	III [G-quartet nanofiber]	356	475	9.42	10^{-2}, Ref.[82]
Ag clusters	III [zeolite assembly]	360	520	N	10^{-2}, Ref.[60]
Carbon dots	III [L-/D-GAm assemblies]	350-370	445-455	N	10^{-3}, ref.[54]
Carbon dots	III [L-/D-GAm assemblies]	380	546, 604	30-55	10^{-3}, Ref.[55]
Carbon dots	III [cellulose nanocrystal assembly]	N	450-620	5.2 (FL), 0.16 (Phos)	10^{-1}, Ref.[52]
2. Chiral inorganic host-based CPL					
Tb^{3+}	III [helical silica]	230	545	N	10^{-3}, Ref.[70]
$CsPbBr_3$	III [helical silica]	365	517.5	N	10^{-3}, Ref.[73]
Tetraphenylethylene (TPE) derivative	III [helical silica]	366	453	57	10^{-2}, Ref.[75]
TPE derivative	III [helical silica]	365	500	20-27	10^{-3}-10^{-4}, Ref.[74]
Tb_2O_3, Eu_2O_3	III [chiral silica nanofibers]	375	545 (Tb_2O_3), 615 (Eu_2O_3)	N	10^{-3}, Ref.[71]
Porphyrin (TCPP), TPE, $MAPbBr_3$	III [chiral silica nanofibers]	375	650 (TCPP), 476 (TPE), 525 ($MAPbBr_3$)	N	10^{-3}, Ref.[72]
Eu^{3+}	III [$TbPO_4{\cdot}H_2O$]	365	590-705	N	10^{-3}-10^{-2}, Ref.[26]
DACT and TMD	III [assemblies of GdOOH nanowires]	N	550 (DACT), 650 (TMD)	N	N, Ref.[76]

N: Not given; FL: fluorescence; Phos: phosphorescence.

luminescence in the visible range. Some typical applications are displayed, followed by a short conclusions and perspectives section.

CONSTRUCTION STRATEGIES FOR CPL-ACTIVE SYSTEMS

There are various strategies to achieve CPL in chiral systems. A straightforward strategy [type I, Figure 2A] is where the luminophore itself is chiral, which is known as an intrinsically chiral luminophore. However, unlike organic molecules with diverse chiral geometries, many inorganic luminescent substances are not chiral. Therefore, a subtle design of symmetry-breaking synthetic methods is often required to produce chiral structures[26,29]. Chirality transfer is widespread on various interfaces[30,31], which makes it more flexible and versatile to enable CPL, even on preformed achiral luminophores. More specifically, the chirality can be transferred from chiral ligands [type II, Figure 2B] and chiral hosts [type III, Figure 2C]. In Type I, to acquire chiral products, chiral ligands or hosts are also employed but are finally removed. Compared with type I, one characteristic in types II and III is that the chiral ligands or hosts are required to co-exist with the luminophore for chirality inducement.

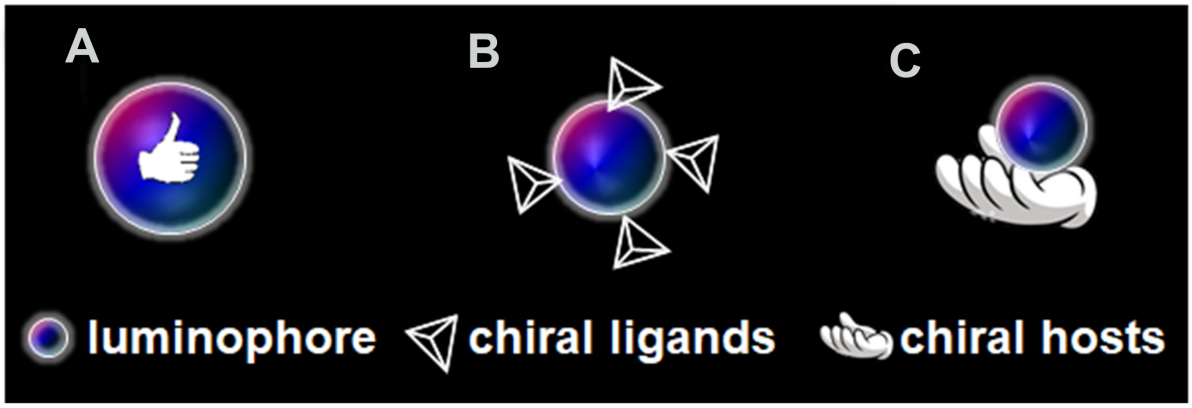

Figure 2. Three types of construction strategies of CPL-active systems: (A) intrinsically chiral luminophores (type I); (B) chiral ligand-induced CPL (type II); (C) "host-guest"-induced CPL (type III). CPL: Circularly polarized luminescence.

Intrinsically chiral luminophores (type I)

The chirality in inorganic materials can appear in various forms. For crystalline materials, point and space groups are basic tools to describe crystal structures. There are 230 group spaces, which are created via the combination of 32 point groups and 14 types of Bravais lattices. Point and space groups are also useful to judge chirality and chiroptical activity. Chiral crystals can exist in 65 Sohncke space groups, which are divided into two categories: I) 22 chiral groups with helical operations that thus contain 11 enantiomeric pairs (e.g., $P3_1$ and $P3_2$); II) the remaining 43 groups are achiral; however, if the unit (i.e., the smallest collection of atoms from which the whole crystal is restored by the application of all symmetry operations of the space group and translation) is chiral, the crystals can be chiral[32]. Early in 1948, chiral crystals with CPL activity were demonstrated in sodium uranyl acetate $Na[UO_2(CH_3COO)_3]$ crystals formed from achiral molecular subunits. The space group of $Na[UO_2(CH_3COO)_3]$ crystals belongs to the chiral space group of $P2_13$ and the chirality is caused by the helical canting of the three $[UO_2(CH_3COO)_3]$ rings and the noncentrosymmetric spatial arrangement of four coordination clusters. Moreover, the crystallographic structure is cubic, which is advantageous to observe CPL with small interruptions caused by birefringence. With such unique structures, a high g_{lum} of 1.31 was observed in $Na[UO_2(CH_3COO)_3]$ crystals by Riehl and Richardson[33] and Moran *et al.*[34].

Another method to endow crystals with optical activity is by creating crystalline defects (e.g., screws and distortions), which are caused by chiral additives regulating the nucleation-growth process[35]. In addition to the lattice chirality described above, chiral nano-/micromorphologies (e.g., copying the helical patterns of chiral organic templates) on a higher length scale can also induce chiroptical activity in crystalline or amorphous materials[31]. Duan *et al.*[36] demonstrated chiroptically-active crystalline ZnO films with multiple chiralities on different scales. Using chiral amino acids of L-/D-methionine (Met) as both structure-directing and symmetry-breaking agents, chiral hydroxide zinc carbonate (HZC) nanostructures were formed on quartz substrates. After removing organic species by calcination at 550 °C in air, HZC was transformed into chiral nanostructured ZnO films (L-CNZF, obtained with L-Met) with three levels of chirality [Figure 3]. On the primary level, the crystal structure of the ZnO nanoplate shows a subtle helical distortion along the [10-11] axis in a left-handed coiled pattern together with some lattice defects, which is caused by the chiral center of the methionine molecules. On the secondary level, several dozens of ZnO nanoplates are bent into a ZnO particle with a right-handed helix form. On the tertiary level, the arrangement of several ZnO particles forms a left-handed circinate helical morphology on the microscale. For the ZnO films (D-CNZF) obtained using D-Met, the handedness one of each level is just opposite to the corresponding one of L-CNZF. These ZnO films showed various chiroptical activities in their CD, CPL and

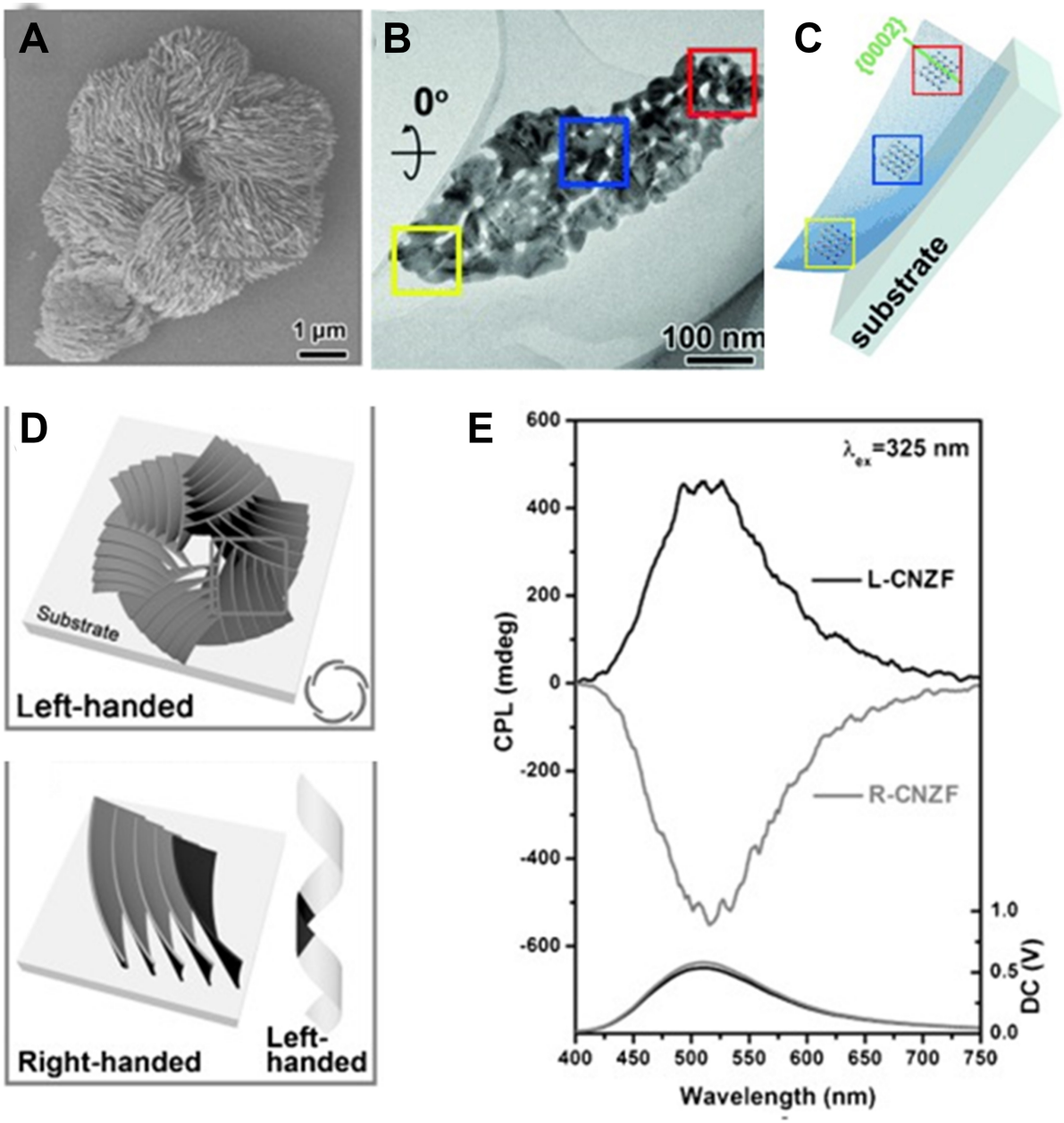

Figure 3. (A) SEM image of L-CNZF. (B) TEM image and (C) SAED patterns of a single ZnO nanoplate. (D) Schematic of hierarchical chirality in L-CNZF. (E) PL and CPL spectra of L- and R-CNZF. Reproduced with permission from Ref.[36]. Copyright (2015) John Wiley and Sons. SAED: Selected area electron diffraction; CPL: circularly polarized luminescence; PL: photoluminescence; CNZF: chiral nanostructured ZnO films.

Raman optical activity spectra. Under a 325 nm excitation, D-CNZF and L-CNZF exhibited antipodal CPL signals centered at 510 nm, consistent with the fluorescence band maximum.

Chiral ligand-induced CPL (type II)

Small chiral organic molecules are widely found and are powerful for producing chiroptical signals on inorganic substances. As shown in Figure 4, for example, CD signals are observed on plasmonic metal (Au and Ag) and semiconductor (e.g., CdS, CdSe and CdTe) NPs capped with chiral ligands[40-42]. The chirality

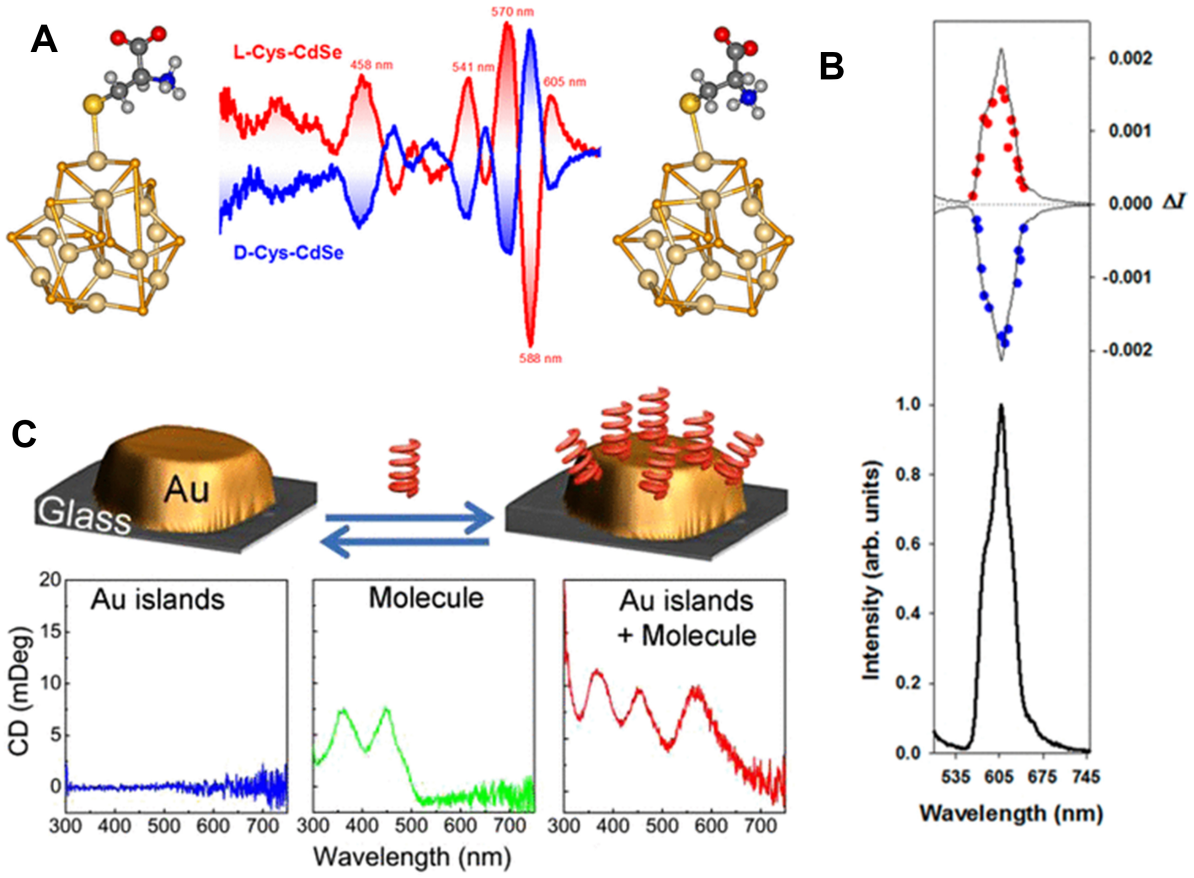

Figure 4. (A) Optimized geometries and induced CD spectra. (B) CPL (top) and total luminescence (bottom) spectra of L- and D-cysteine-capped CdSe quantum dots. Reproduced with permission from Ref.[41]. Copyright (2013) American Chemical Society. (C) Chiral riboflavin molecule-induced CD optical activity in Au islands deposited on a glass substrate. Reproduced with permission from Ref.[42]. Copyright (2013) American Chemical Society. CD: Circular dichroism; CPL: circularly polarized luminescence.

transfer from ligands to inorganics can proceed through various mechanisms, including surface atom distortion with asymmetric clusters, the chiral arrangement of ligands on the surface, crystalline defects and the electronic interaction or coupling between chiral molecules and inorganic species[43,44].

The combination between inorganic nanomaterials and chiral ligands can be fulfilled by two synthetic routes, namely, ligand-guided one-step synthesis or post-modification by ligands exchanges. Although these methods appear easy to carry out, the chirality induction is dependent upon many factors, such as the types of ligands, the sizes/shapes of the NPs and the synthetic conditions. Furthermore, although the chirality is mainly judged by the CD signals, CD activity does not guarantee CPL activity. This is understandable based on the differences between the CD and CPL mechanisms, i.e., CD is associated with absorption from the ground states, while CPL is associated with emissions in the excited states.

"Host-guest"-induced CPL (type III)

Based on the concept of chirality induction in type II, it is found that various luminescent guests show chiroptical activity after being embedded in many chiral materials as chiral hosts. Moreover, several different guests can be simultaneously integrated into one host to acquire white CPL. In particular, with this method, emerging novel inorganic nanomaterials have found broad applications in CPL in recent years by

encapsulating inorganic and/or organic luminescent guests. As a result, this strategy is more flexible for producing multicolor CPL by a rational combination between hosts and guests, thus widening the scope of inorganic CPL-active systems.

OVERVIEW OF INORGANIC-ASSOCIATED CPL-ACTIVE SYSTEMS

Inorganic luminophore-containing systems

Metal ion-based luminophores

Lanthanide ions [Ln(III)] are appealing for CPL because of their interesting optical properties, such as a large pseudo-Stokes shift, long lifetime and unique spectral fingerprint from the ultraviolet (UV) to near-infrared (NIR) range. In particular, the magnetic dipole allowed transitions in lanthanide ions are advantageous for a high g_{lum}; for example, a high g_{lum} value of 1.38 was reported for Eu(III) complexes[45]. Since lanthanide ions are isotropic, lanthanide-based CPL is predominantly demonstrated in various chiral lanthanide complexes, where the coordination orientation of chiral ligands can form left- or right-handed twists and helices. The CPL mechanism of these complexes can be interpreted based on multipole [Ln(III)]-point charge (chiral ligand) interactions and/or multipole [Ln(III)]-dipole (excited-ligand) coupling. Since there have been several recent reviews on CPL-active lanthanide complexes, they are not described here and the reader can refer to Refs.[46-48].

Other transition metal complexes with CPL activity have also been reported. For example, chromium(III) (Cr^{3+}) is of interest due to its earth abundance, kinetic inertness and magnetically allowed but electric-dipole forbidden emissions (600–800 nm) from the Cr(^{2}E) and Cr($^2T_1$) states. In a recent report, helical $[Cr(dqpR)_2]^{3+}$ (dqp = 2,6-di(quinolin-8-yl)pyridine; R = OCH_3, Br or C ≡ CH) complex enantiomers were resolved[49]. A high quantum yield (up to 17%), long-lived excited lifetimes (1.35 ms) at room temperature in aqueous solutions and a large g_{lum} (0.20) were found for these chiral complexes, thereby providing satisfactory CPL brightness. More reports on CPL-active chromium-based materials have been well summarized in a recent review[50], so this topic will not be discussed in detail here.

In addition to metal complexes, metal ion-containing luminophores can also be found in metal oxides (e.g., Eu_2O_3) and metal ion-doped inorganic matrixes (e.g., $NaYF_4$:Yb/Tm, $NaYF_4$:Yb/Er and $CaAl_2O_4$:Eu,Nd). As discussed below, they can also be engineered with CPL in highly thermal stable oxides for up-conversion, NIR emission and phosphorescence applications.

Carbon dots

Since the discovery of carbon dots in 2006, their luminescence has gained increasing attention as they possess many important features, such as easy production, rich raw materials, multicolor emission, high stability and versatile surface chemistry. In some early reports, carbon dots with chiroptical activity in their CD spectra were easily prepared using chiral molecular precursors; however, the CPL activity was not easily demonstrated[51]. The CPL of carbon dots was recently activated using the simple "host-guest" strategy[52-55].

One special characteristic of carbon dots is that their emission wavelength can be tuned by changing their excitation wavelength. Building on this phenomenon, Li *et al.*[54] showed an excitation-dependent CPL example. A chiral L-/D-glutamic acid gelator (L-/D-GAm) was assembled into a helical structure that was used as a chiral host to co-assemble with the nitrogen-doped carbon dot guest. The as-formed composites (L-and D-co-gels) appeared as spiral nanotubes [Figure 5A]. The maximum emission wavelength changed from 400 to 460 nm as the excitation wavelength increased from 300 to 400 nm [Figure 5B]. Similarly, the CPL signals were also red-shifted with increasing excitation wavelength from 350 to 370 nm [Figure 5C] and the $|g_{lum}|$ was ~ 2×10^{-3}-4×10^{-3} under a 360 nm irradiation.

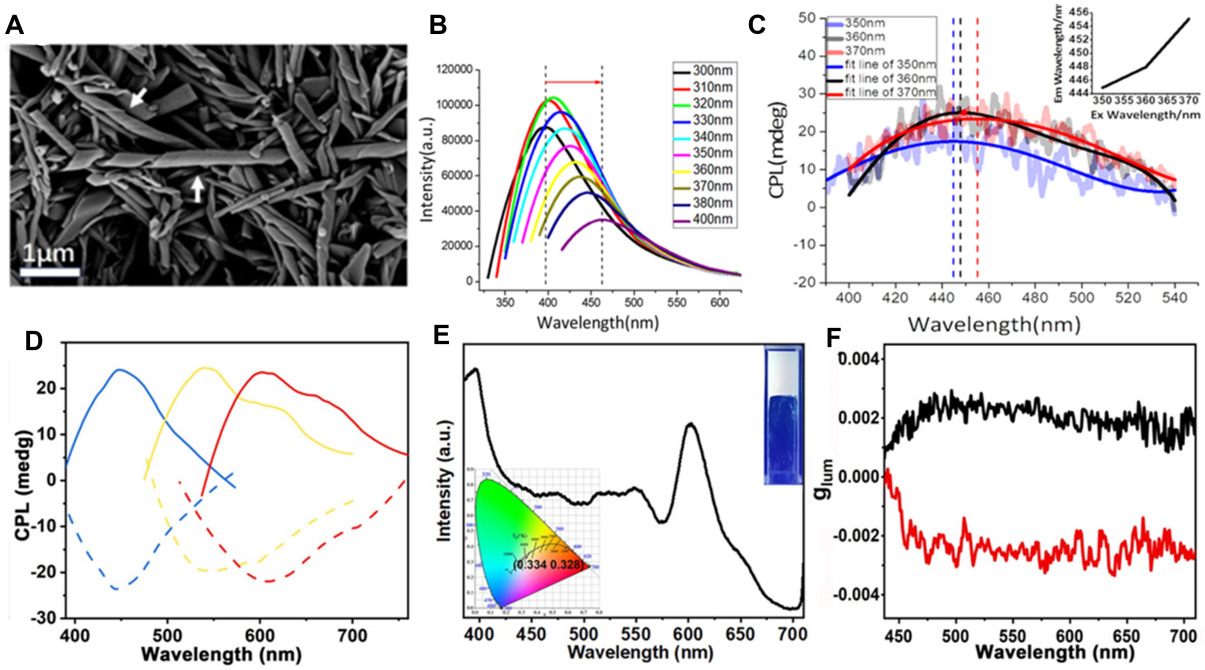

Figure 5. Morphologies and optical properties of D-co-gel: (A) FE-SEM image; (B) PL; (C) CPL spectra with the fitting line (inset: plot of the maximum CPL emission wavelength versus the excitation wavelength) under different excitations. Reproduced with permission from Ref.[54]. Copyright (2020) American Chemical Society. (D) Mirror image CPL spectra of three carbon dot-doped co-gels. (E) PL spectra of white-emitting co-gel (insets: a photograph of the co-gel under 365 nm (top right) and its CIE coordinate value (bottom left). (F) g_{lum} of white-emitting co-gel from D-GAm (black) and L-GAm. Reproduced with permission from ref.[55]. Copyright (2021) John Wiley and Sons. PL: Photoluminescence; CPL: circularly polarized luminescence.

Again, using L-/D-GAm co-gels as the hosts to encapsulate three kinds of carbon dots with blue, yellow and red emission colors, Ru *et al.*[55] demonstrated a white CPL system. These carbon dots displayed CPL signals at 450, 550 and 610 nm, with a $|g_{lum}|$ of ~10^{-2} [Figure 5D]. Furthermore, by simply blending these three kinds of carbon dots at a mass ratio of 4.63:15.75:1 (blue:yellow:red), white emission was fulfilled with a CIE chromaticity diagram coordinate value of (0.334, 0.329) [Figure 5E]. This as-obtained mixture showed circularly polarized white-light emission with a g_{lum} of ~ 2.5×10^{-3} [Figure 5F], which is smaller than the g_{lum} of the individual carbon dots.

Metal clusters

Fluorescent metal clusters composed of a few to a hundred atoms represent a class of special luminophores that provide a link between nanoparticles and the atomic behavior of metals. These ultrasmall metal clusters exhibit molecule-like properties, including size-regulated fluorescence and discrete electronic states, which are promising for a broad range of biological applications. The ultrasmall size of the metal clusters is also possibly advantageous for the combination between metal clusters and ligands (or hosts), meaning that diverse CPL-active metal clusters can be synthesized by the three strategies discussed above (types I-III)[56].

Wu*et al.*[57] synthesized spirocyclic Ag clusters [2-(R) and 2-(S), Figure 6A] using two types of chiral diide ligands and 2-(pyridin-2-yl)-1H-benzo[d]imidazole (PBZ). The intrinsic chirality origin of 2-(R) and 2-(S) can be ascribed to the chiral diides, the spirocyclic arrangement of a Ag_9 cluster and the helical arrangement of PBZ molecules. In addition, 2-(R) and 2-(S) can crystalize into crystals with the chiral space group of $P2_1$. In a mixed solvent of water and methanol, with an increase in the water fraction, 2-(R) and 2-(S) assemble into μm-long helical nanofibers. Furthermore, the solid films of 2-(R) and 2-(S) show strong and mirror-

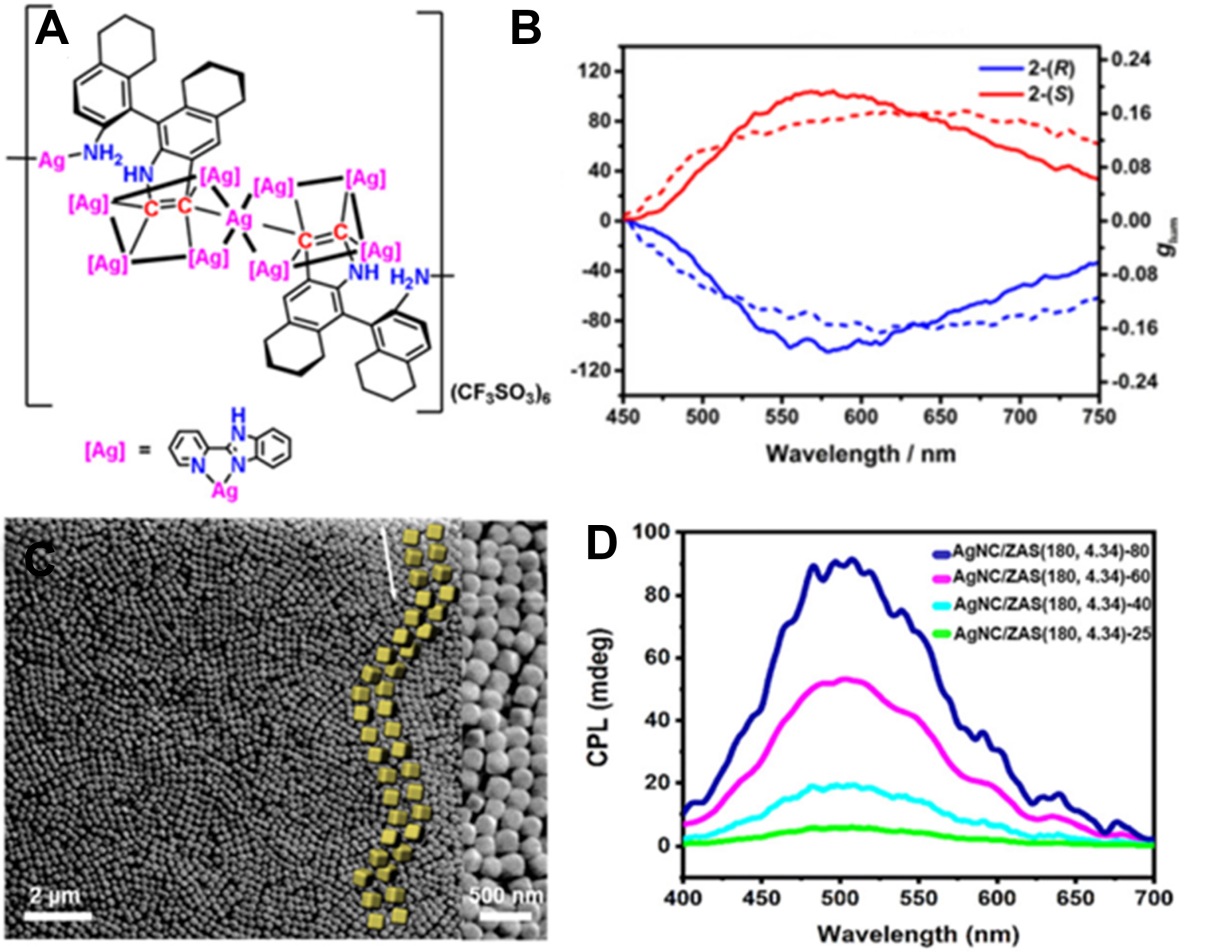

Figure 6. (A) Spirocyclic Ag cluster structure of 2-(S). (B) CPL spectra (solid line) and g_{lum} (dotted line) for film samples of 2-(R) and 2-(S). Reproduced with permission from ref.[57]. Copyright (2021) John Wiley and Sons. (C) SEM image of ZAS(180, 4.34)-80 showing helices with yellow blocks. (D) CPL spectra of AgNC/ZAS(180, 4.34)-T under different temperatures (T). Reproduced with permission from Ref.[60]. Copyright (2020) John Wiley and Sons. CPL: Circularly polarized luminescence; ZAS: zeolite LTA superball.

imaged CPL signals centered at 558 nm, with a high g_{lum} of 0.16 [Figure 6B]. Such a high g_{lum} may benefit from the exciton couplings between the helically arranged PBZ molecules of individual spirocyclic clusters and the microscopic helical assembly. In other words, both the molecular-level and microscale chirality contribute to the high g_{lum}. The assembly- and aggregate-induced CPL of metal clusters is also found in gold clusters of Au_3[R/S-BINAP]$_3$Cl and copper clusters of $[Cu_{14}(R/S\text{-DPM})_8]^{6+}$ (DPM = R/S-2-diphenyl-2-hydroxylmethylpyrrolidine-1-propyne), which are CPL inactive when dispersed in good solvents (e.g., CH_2Cl_2) but become CPL active in the aggregate states after the addition of poor solvents (e.g., n-hexane)[58,59].

Using a host-guest method, Tao *et al.*[60] reported the CPL activity of luminescent Ag nanoclusters (AgNC) incorporated in colloidal zeolite LTA superball (ZAS) assemblies. The macroscopic porous films built from ZAS showed 3D long-range periodicity featuring a photonic band gap (PBG) [Figure 6C]. For one-dimensional PBG structures, the maximum PBG wavelength λ_{max} is calculated as follows: $\lambda_{max} = nP\sin\theta$, where n and P are the average refractive index and helical pitch of a PBG structure, respectively, θ is the angle of the incident light with respect to the PBG structures. A PBG structure with a helical periodic profile can selectively reflect CP light, especially at λ_{max}, with the same handedness of the PBG structure while

allowing the transmittance of the opposite-handed CP light[61-63]. For example, LCP is blocked while RCP is transmitted within a left-handed helical PBG structure, and therefore a large difference between LCP and RCP was detected with a high g_{lum}. By embedding luminescent AgNC, the AgNC/ZAS enabled the selective reflection of R-CP light and allowed L-CP light, resulting in a g_{lum} of 0.013 at a 520 nm emission. The g_{lum} can be tuned by the assembly temperature to change the helical pitches of PBG structures [Figure 6D].

Semiconductor nanocrystals

Semiconductor nanocrystals (NCs), mainly comprised of elements from the II-VI, III-V and IV-VI groups of the periodic table, show many promising optical properties, including exceptional brightness, high quantum yield, superior photostability and size-tunable emission. Colloidal semiconductor NCs are usually capped with organic ligands for the purposes of surface passivation and good dispersibility. In addition, surface ligands also influence the photoluminescent properties. By a ligand-exchange step, chiral ligands can be absorbed onto the surfaces of NCs to make semiconductor NCs CPL active[27,41,64].

As shown in the previous work by Tohgha *et al.*[41], CPL signals at ~ 605 nm ($|g_{lum}|$ of 3-4×10^{-3}) are observed on CdSe NPs modified with D- and L-cysteine. Furthermore, Cheng *et al.*[64] conducted a systematic study of the CPL properties of cysteine-modified CdSe/CdS core-shell NCs with different shapes [Figure 7A][27]. The CdS shell could improve the luminescent quantum yield (QY) of the CdSe core. Interestingly, even if the CdSe core is separated from chiral ligands by the CdS shell, CdSe still shows CPL bands from 550 to 650 nm with a $|g_{lum}|$ of 1-9×10^{-4}. The CPL performance may be caused by orbital coupling and Coulombic dipole interactions between CdSe and cysteine. The PL and CPL could be manipulated by the thickness and shapes of the CdS shell (g_{lum} increases with decreasing CdS shell thickness) but is proportional to the QY [Figure 7B and C]. This work confirmed that chiral ligands can control the whole wavefunction even though there exists an energy barrier of the thin CdS shell.

Perovskite nanocrystals

Luminescent metal halide perovskite colloidal NCs composed of inorganic octahedral layers and organic ligands represent a class of promising next-generation optoelectronic materials. As summarized in recent reviews[65-67], using type I and II strategies with the assistance of a series of chiral ligands, CPL is also extended to perovskite NCs with potential applications in CP light detection, quantum networks, ferroelectrics and spintronics. In addition to organic molecules as chirality sources, some inorganic nanomaterials are also able to endow perovskite NCs with CPL activity, thereby offering new CPL-active candidates.

Chiral inorganic host-based systems

Chiral silica

Over the past two decades, a variety of chiral silica nanomaterials have been reported and their chirality can be manifested by helical outwards or molecular-scale asymmetry on the siloxane framework[68]. Compared with chiral organic molecules, a prominent feature of silica is its thermal stability (close to 1,000 °C), which is desirable for high-temperature synthetic procedures. It has been confirmed that ions, molecules and nanoparticles incorporated within these chiral nano-silica materials can become CD active[69,70]. With the above success, it is of interest to explore chiral silica-based CPL-active systems.

Our group first demonstrated several entirely inorganic silica-lanthanide oxide CPL systems[71]. In our previous work, we found that linear polyethylenimine and L- (or D-) tartaric acids can co-assemble into catalytic chiral templates to direct the formation of chiral SiO_2 nanofibers [Figure 8A]. Vibrational circular dichroism spectroscopic analysis revealed the asymmetric feature of Si-O-Si frameworks on the molecular

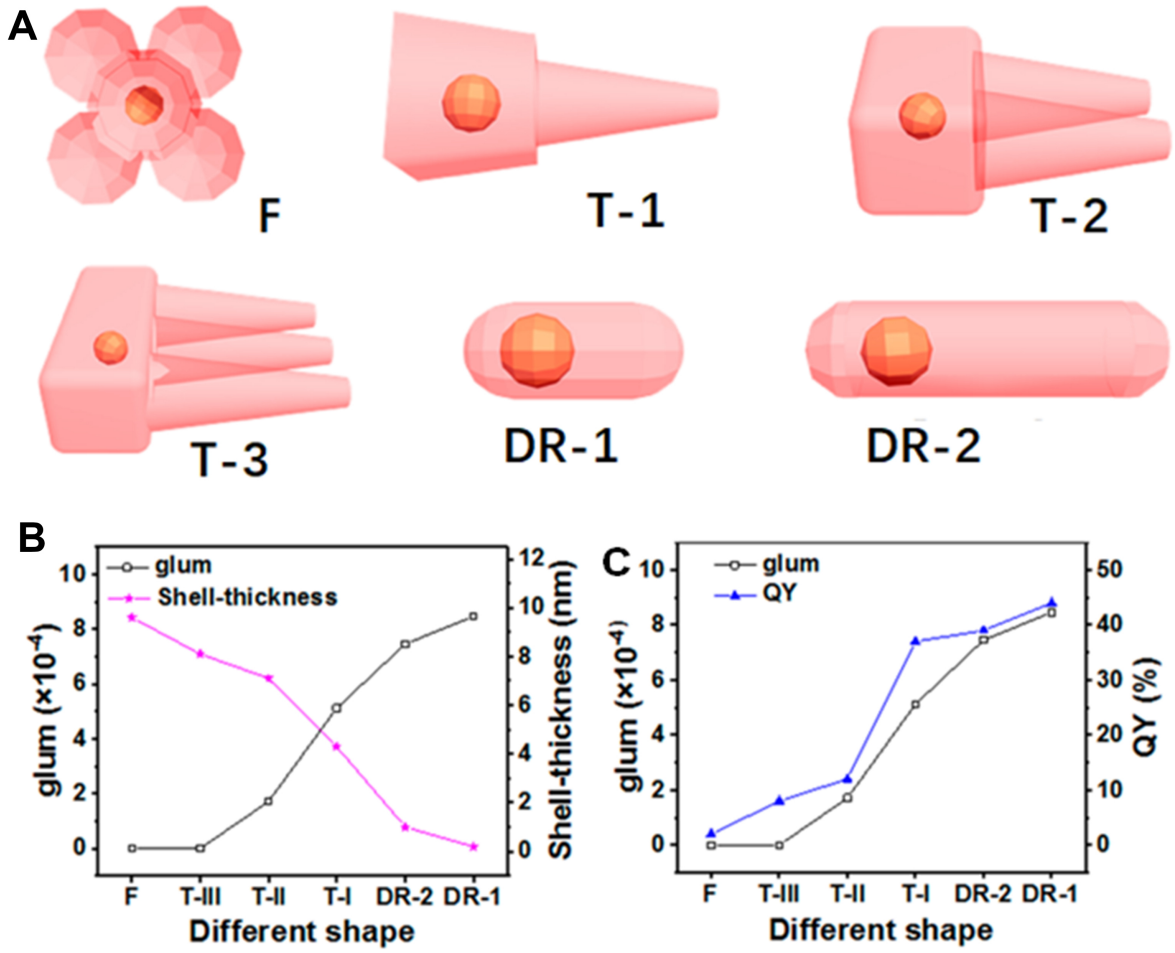

Figure 7. (A) Schematic anisotropic shapes of CdSe/CdS (gold-colored core: CdSe; orange-color shell: CdS). (B) Dependence of g_{lum} of D-Cys-CdSe/CdS, CdS shell thickness and (C) QY on different shapes. Reproduced with permission from Ref.[27] Copyright (2020) American Chemical Society. QY: Quantum yield.

scale, which can be maintained even up to 900 °C. These SiO_2 nanofibers are used as chiral nanoreactors for the formation of sub-10 nm Eu_2O_3 (or Tb_2O_3) NPs, which are transformed from the Eu^{3+} (or Tb^{3+}) trapped in SiO_2 after heating at 900 °C in air [Figure 8B and C]. Interestingly, the CPL features of NPs are observed around the emission wavelengths of 615 nm (Eu_2O_3) and 545 nm (Tb_2O_3) with a $|g_{lum}|$ of the order of 10^{-3}. However, the excitation wavelength using homemade CPL spectroscopy is 375 nm, which deviates from the optimized excitation wavelength from PL spectra. The influence of the excitation wavelength on the CPL performance was not probed.

In addition to lanthanide oxides, other luminophores are also endowed with CPL after being embedded within these SiO_2 nanofibers [Figure 8D][72]. As a unique luminescent phenomenon, aggregation-induced emission (AIE) has gained ever-increasing attention. Tetraphenylethene (TPE) and its derivatives are representative AIE luminogens (AIEgens) with high quantum yields and ready functionalization. TPE molecules can be easily absorbed onto SiO_2 nanofibers modified with phenyl groups and have already demonstrated AIE-based CPL signals of ~ 476 nm in the aggregated state. When SiO_2 was modified by amine groups, fluorescent carboxylic molecules (5,10,15,20-tetrakis(*P*-carboxyphenyl)porphyrin, 1-

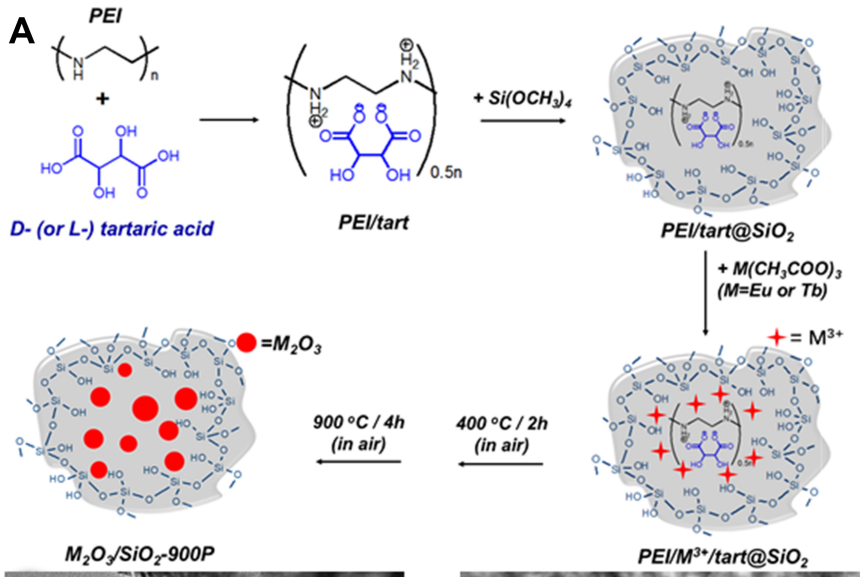
A
PEI
D- (or L-) tartaric acid
PEI/tart
+ Si(OCH3)4
PEI/tart@SiO2
+ M(CH3COO)3
(M=Eu or Tb)
= M3+
PEI/M3+/tart@SiO2
400 °C / 2h
(in air)
900 °C / 4h
(in air)
=M2O3
M2O3/SiO2-900P

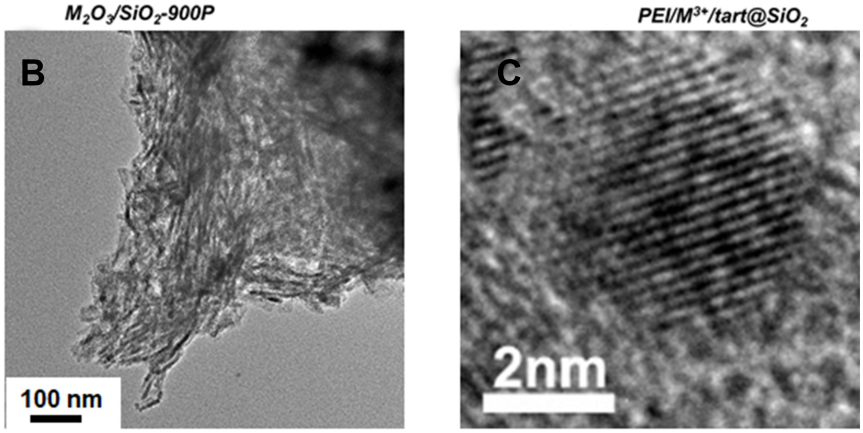
B
100 nm
C
2nm

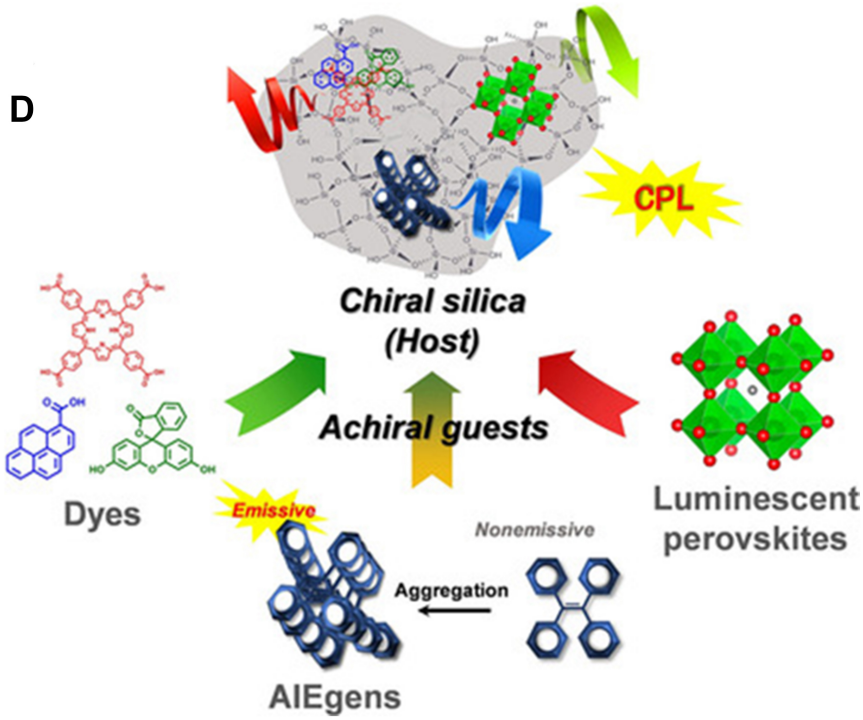
D
CPL
Chiral silica
(Host)
Achiral guests
Dyes
Luminescent
perovskites
Emissive
Nonemissive
Aggregation
AIEgens

Figure 8. (A) Schematic of chiral SiO_2 nanofiber synthesis using PEI/D-tart (or PEI/L-tart) as chiral catalytic templates and their usage to prepare chiral lanthanide oxide (M_2O_3) NPs. (B) TEM image of Tb_2O_3/D-SiO_2 nanofibers. (C) TEM image of an individual Tb_2O_3 nanoparticle on Tb_2O_3/D-SiO_2 nanofibers. Reproduced with permission from Ref.[71]. Copyright (2018) John Wiley and Sons. (D) Various CPL-active systems using chiral silica as hosts to incorporate organic fluorescent dyes, AIEgens and perovskites NCs. Reproduced with permission from Ref.[72]. Copyright (2020) John Wiley and Sons. CPL: Circularly polarized luminescence.

pyrenecarboxyl acid and fluorescein) were attached to SiO_2 and then showed CPL signals at their characteristic emission bands with a $|g_{lum}|$ of 2-5×10^{-3}. In addition, these amine-modified SiO_2 materials could work as chiral reactors for the *in-situ* formation of perovskite NCs with CPL activity. These results imply the significant potential of chiral SiO_2 in designing CPL-related materials.

Harada *et al.*[70] found that cationic gemini surfactants of C_2H_4-1,2-$[(CH_3)_2N^+C_{16}H_{33}]_2$ self-assemble into helical structures in the presence of L- or D-tartrate counter ions. Using these organic helices as templates (dented by 16-2-16 L-tartrate or 6-2-16 D-tartrate), elegant right- and left-handed SiO_2 nanohelices could be prepared and further used as chiral hosts to synthesize lanthanide ion- and perovskite-containing CPL systems [Figure 9A]. After the absorption of Tb^{3+} onto SiO_2 nanohelices and calcination at 900 °C for 4 h in air, the small amount of Tb^{3+} (~ 0.31%) can display CPL outputs at ~ 545 nm (irradiated at 230 nm) with a $|g_{lum}|$ of ~ 10^{-3} due to the helical-morphological chirality of SiO_2. The chiroptical activity may be due to the 4f orbitals of Tb^{3+} being chirally distorted by the asymmetrically arranged Si-O framework. In addition, after modifying the surfaces of SiO_2 helices with amine by 3-aminopropyl-triethoxysilane, perovskite $CsPbBr_3$ nanocrystals (PNCs) are grafted onto SiO_2[73]. When suspended in toluene, PNC-SiO_2 do not exhibit CD and CPL signals. In contrast, after casting the above suspension on quartz and drying, the PNC-SiO_2 in a dried film state became both CD and CPL active. The maximum CPL signals locate at 517.5 nm (under a 360 nm excitation) and the $|g_{lum}|$ reaches 5.7-6.9×10^{-3}. It was found that PNCs are closely packed and helically arranged around SiO_2 helices during the solvent evaporation process, which facilitated the dipolar interaction between the PNCs and then produced CPL.

The synthesis of the CPL-active materials above occurs via a two-step process, which requires the synthesis of SiO_2 in advance. In fact, the luminescent components could also be one-step incorporated into a siloxane framework during the condensation of silica sources (e.g., tetraethyl orthosilicate and multisilylated organic molecules). For example, Cai *et al.*[74] designed TPE-containing bis(triethoxysilane) (BTSTPE) as the silica precursor and then prepared TPE-bridged polybissilsesquioxane (TPE-silica) nanotubes with single-handed helicity using the self-assemblies of a pair of chiral cationic low-molecular-weight gelators (L-ValPyBr and D-ValPyBr) as templates [Figure 9B]. Strikingly, the TPE-silica products showed high thermal stability with only a 5% weight loss at ~ 500 °C. The helical TPE-silica powders emit green light at ~ 500 nm with a quantum yield of over 21%, which is higher than that of its precursor of BTSTPE. The CPL outputs are found at 500 nm with a $|g_{lum}|$ of 0.6-1.6×10^{-3}. In another work, Zhang *et al.*[75] reported AIEgen-silica helical nanotubes displaying CPL signals at 453 nm with a g_{lum} up to 0.02 [under a 366 nm excitation, Figure 9C]. The CPL-active products were obtained by the co-assembly from 2-[4-(1,2,2-triphenylethenyl)-phenoxy]-acetic acid (as the luminophore), N-trimethoxysilylpropyl-N,N,N-trimethylammonium chloride (as a co-structure directing agent) and tetraethylorthosilicate (as a silica precursor).

Other chiral inorganic hosts

As discussed above, there are 22 chiral space groups in crystal structures, providing the possibility of generating intrinsically chiral crystalline materials. For example, the space groups of $TbPO_4·H_2O$ crystals belong to the chiral group of $P3_121$ or its enantiomorph $P3_221$. Hananel *et al.*[26] employed tartaric acid enantiomers as chirality inducers to produce chiral $TbPO_4·H_2O$ doped with Eu^{3+}. Under a 365 nm excitation, Eu^{3+} in the $TbPO_4·H_2O$ host showed strong CPL signals between 590 and 720 nm corresponding to the $^0D_5$→

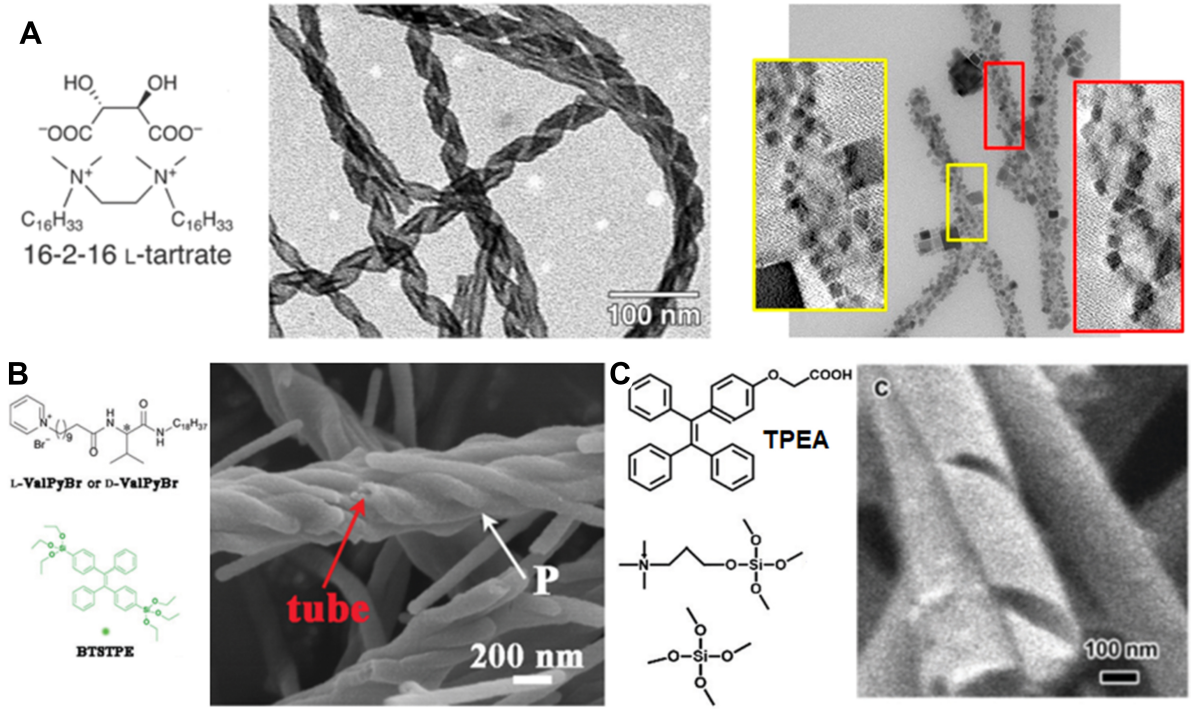

Figure 9. (A) Molecular structure of 16-2-16 L-tartrate (left) and TEM images of L-SiO_2:Tb^{3+} calcined at 900 °C (middle) and nanohelices@PNCs in a dried film and the cross sections (yellow and red frames) obtained with 3D tomography reconstructions (right). Reproduced with permission from Ref.[70]. Copyright (2021) Royal Society of Chemistry. Reproduced with permission from Ref.[73]. Copyright (2020) American Chemical Society. (B) SEM image of TPES-P. Reproduced with permission from Ref. [74]. Copyright (2019) Royal Society of Chemistry. (C) SEM image of L-CASN. Reproduced with permission from Ref.[75]. Copyright (2019) Royal Society of Chemistry. TPES-P: TPE-silica with plus helice. L-CASN: left-handed chiral lamellar mesostructured AIEgen-silica hybrid hollow nanotubes;

^7F_J transitions of Eu^{3+}. The g_{lum} could be 0.06 at 612 nm and is comparable with many chiral Eu(III) complexes. In this work, CPL spectroscopy is also used as a tool to study the symmetry breaking behavior of chiral $TbPO_4 \cdot H_2O$ crystals controlled by the enantiomeric excess (e.e.) of tartaric acid.

Unlike the case above where the symmetry breaking is regulated by chiral molecules, Zhang *et al.*[76] found that oleyamine-coated GdOOH nanowires with a diameter of less than 1 nm could randomly transform into macroscopic left- and right-handed helical assemblies (MHAs) at the centimeter level by an evaporation-induced self-assembly process without the assistance of a chiral dopant [Figure 10A,B][76]. The spontaneous formation of helices is a result of an energy-minimizing process and the handedness is uncontrollable. Fortunately, the left- and right-handed helices can be observed by the naked eye and easily separated. Achiral fluorescent molecule guests of DACT and TMD embedded into MHAs showed CPL signals at their emission bands at 500 and 625 nm, respectively.

SELECTED SPECIAL CPL-ACTIVE SYSTEMS

Many luminophores show down-conversion fluorescence with emission bands in the visible range. In fact, there are other luminescent processes, including up-conversion PL, phosphorescence, thermally activated delayed fluorescence (TADF) and NIR emission. Studies of the CPL related to these processes could enrich our understanding of the origin of CPL and help us to explore more CPL-related applications. Therefore, some special CPL-active systems are presented in this section.

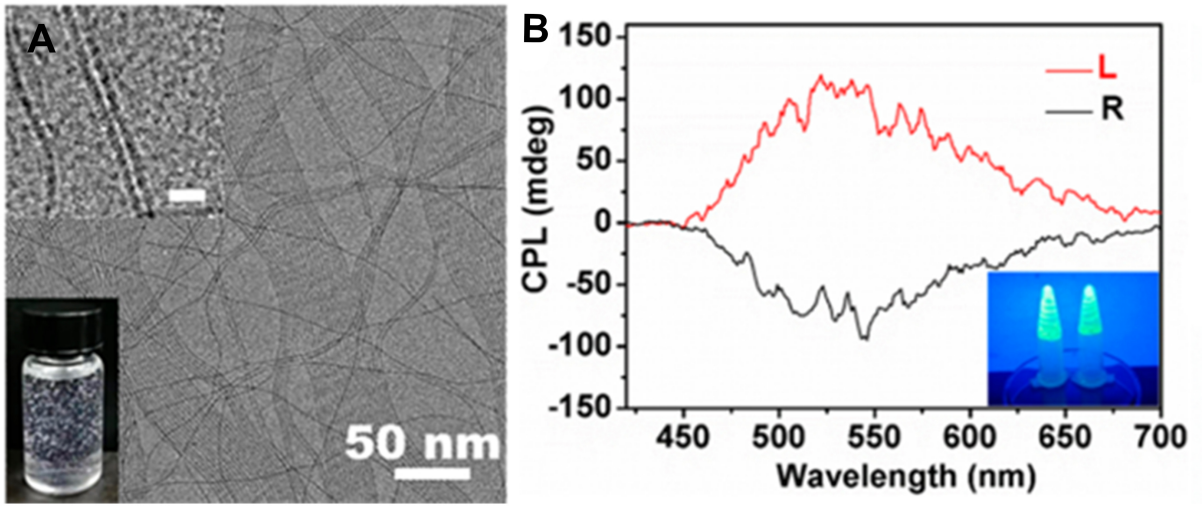

Figure 10. (A) Cryo-electron microscopy image and its large-magnification version (upper inset) of the sub-1 nm GdOOH nanowires (bottom: a photograph of the dispersion of nanowires). (B) CPL spectra of DACT-MHA. Reproduced with permission from Ref.[76]. Copyright (2020) American Chemical Society. CPL: Circularly polarized luminescence; MHA: macroscopically spiral assemblies.

Up-conversion CPL

Up-conversion luminescence is capable of converting long-wavelength NIR light to shorter-wavelength narrow and sharp emission ranging from UV, to visible and even to shorter NIR light. Up-conversion luminescence is utilized widely in a broad range of areas, especially in biological and biomedical ones, due to low background fluorescence, weak photodamage, good penetration in tissues and high sensitivity.

Lanthanide ions (e.g., Yb^{3+}, Er^{3+} and Tm^{3+}) doped in fluoride-based matrixes (e.g., $NaYF_4$ and $NaGdF_4$) possess high up-conversion efficiencies because of sufficient metastable energy and excited states with a long lifetime. Yang *et al.*[77] offered a dexterous solution for an up-conversion CPL based on a radiative energy transfer process from $NaYF_4$:Yb/Tm Upconverting nanoparticles (UCNPs) to $CsPbBr_3$ perovskite nanocrystals (PKNCs) in the chiral nematic liquid crystal (N*LC) featured with PBG [Figure 11A]. A high $|g_{lum}|$ is possible in a PBG structure due to strong handedness-selective reflection of CP light. However, the light loss may occur and the emission of emitters is boosted when the emission wavelength is located at the edge of the photonic bandgap, while the emission is suppressed at the center of the bandgap. Therefore, it is a challenge to achieve both a large g_{lum} and high emission efficiency. To address this issue, an achiral nematic liquid crystal SLC1717 and chiral dopant R-(or S-)811 were used to form left- or right-handed helical N*LC, where two different emitters of $NaYF_4$:Yb/Tm and $CsPbBr_3$ were embedded. Under a 980 nm excitation, $NaYF_4$:Yb/Tm UCNPs showed emission bands at 450 and 475 nm near the edge of the bandgap of N*LC and these emissions were thus enhanced and the g_{lum} at 475 nm was 0.3. The emission of PKNCs was centered at 495 nm, which overlaps with the center of the bandgap. Fortunately, the emission of PKNCs could be enhanced via a radiative energy transfer with quenching the emission of $NaYF_4$:Yb/Tm at 475 nm. Meanwhile, a very high g_{lum} of 1.1 was still achieved for PKNCs at 495 nm.

NIR emission CPL

The emission at the NIR range from luminophores is highly beneficial to optical applications in transparent biological windows because of the suppressed absorption or scattering from skin and blood. However, there is a lack of suitable, reliable detection instruments for weak NIR emission and reports on NIR-CPL are scarce. Yb^{3+} is a typical NIR emitter in the range of 900–1050 nm. The complex of $Yb(TTA)_3$ (TTA = 2-thenoyltrifluoroacetonate) shows relatively good quantum yields due to the antenna effect of TTA ligands.

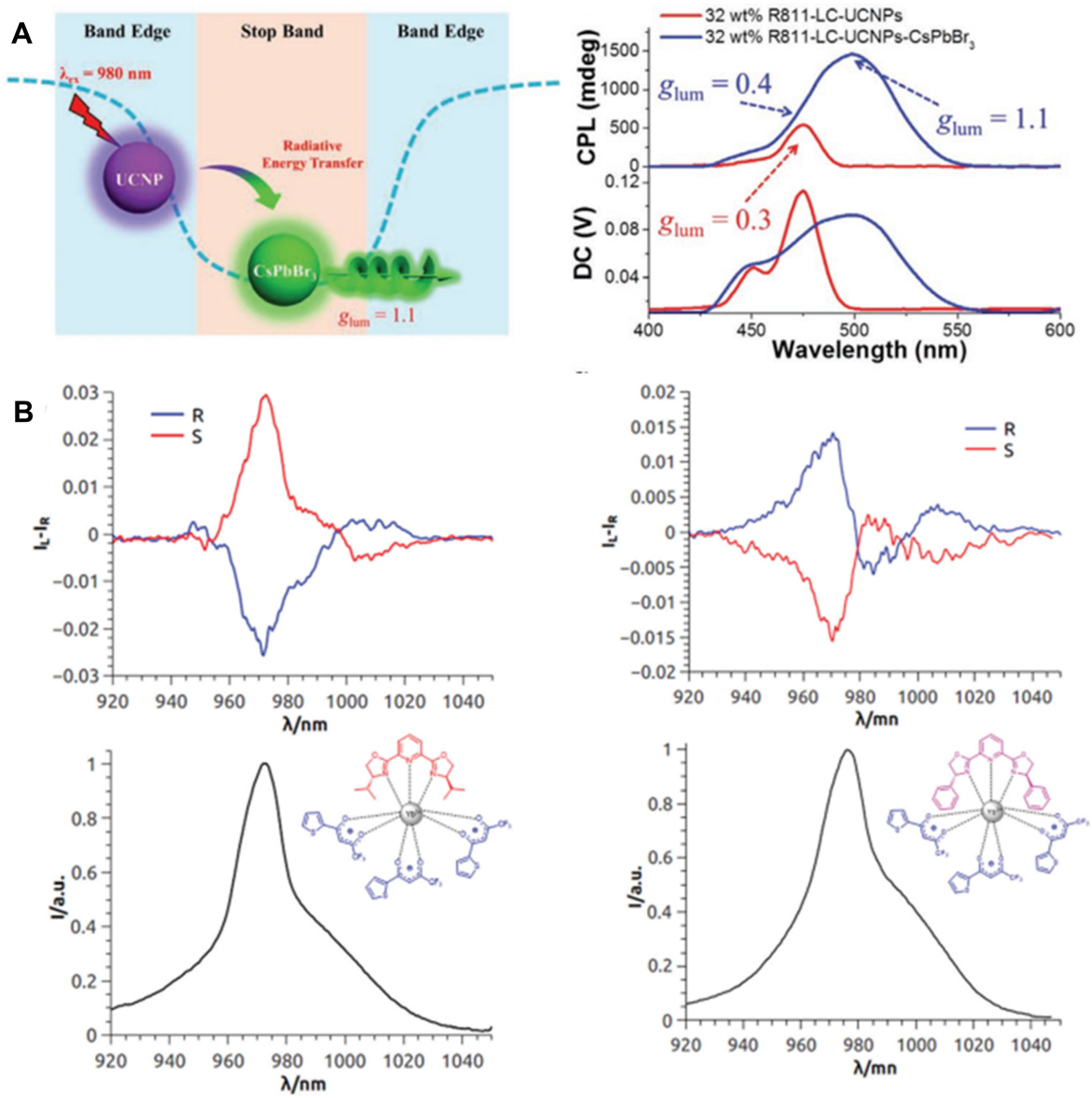

Figure 11. (A) Schematic representation of RET process from UCNPs to $CsPbBr_3$ PKNCs in N*LC (the emissions of $CsPbBr_3$ PKNCs and UCNPs were located at the center and the edge of the photonic bandgap, respectively, left) and UC-CPL spectra of $CsPbBr_3$ PKNCs/UCNPs in N*LC with di erent incident power of a 980 nm laser (right). Reproduced with permission from Ref.[77]. Copyright (2020) John Wiley and Sons. (B) NIR-CPL spectra (top) of both the enantiomers of $Yb(TTA)_3{}^{i}PrPybox$ (left) and $Yb(TTA)_3PhPybox$ (right) and total NIR emission (bottom). Reproduced with permission from Ref.[78]. Copyright (2019) Royal Society of Chemistry. RET: Radiative energy transfer; PKNCs: perovskite nanocrystals; UCNP: upconverting nanoparticles; TTA: 2-thenoyltrifluoroacetonate.

On the basis of $Yb(TTA)_3$, Zinna *et al.*[78] introduced additional chiral ligands ($^{i}PrPyBox$ or PhPyBox) to synthesize two groups of chiral $Yb(TTA)_3{}^{i}PrPyBox$ and $Yb(TTA)_3PhPyBox$ complexes [Figure 11B]. To measure the NIR-CPL of these complexes, the authors conducted modifications on spectrofluoropolarimeter apparatus using an Ag-O-Cs photomultiplier tube as the detector and a photoelastic modulator coupled with an uncoated Glan–Thompson polarizer for polarization discrimination. For $Yb(TTA)_3{}^{i}PrPyBox$, relatively sharp peaks at 972 nm ($^2F_{5/2} \rightarrow {}^2F_{7/2}$ transition of Yb^{3+}) appeared on their CPL spectra appeared with a g_{lum} of -0.025 and +0.029 for (R,R) and (S,S) enantiomers,

respectively. Similar results were also found for $Yb(TTA)_3PhPyBox$ enantiomers.

Thermally activated delayed fluorescence CPL

In principle, TADF enables an internal quantum efficiency of 100% by harvesting triplet (T1) excitons, which is fulfilled through the reverse intersystem crossing from the triplet (T1) to singlet (S1) state in a thermally activated process. Therefore, TADF has received widespread attention, especially in organic light-emitting diode displays. Recently, TADF-based CPL has also gained increasing interest in organic molecules[79]. In contrast, TADF-CPL in inorganic emitters is rare. Han *et al.*[80] synthesized octahedral Ag(I) clusters using chiral ligands named as L/D and PL/PD enantiomers [structures shown in Figure 12A]. In the case of PL/PD, Ag_6 cores in the Ag clusters of Ag_6PL_6 and Ag_6PD_6 are distorted and deviate from the regular octahedral Ag6 skeleton, and these clusters crystallize in the chiral monoclinic space group $P2_1$. Based on chiroptical spectra and DFT simulations, the chiroptical activity of the clusters is mainly attributed to the asymmetric Ag_6 core and the chiral interface between Ag and the coordinated C and N atoms. The PLQY of Ag_6PL_6/Ag_6PD_6 surpasses 95% at room temperature, which is a result of TADF confirmed by the temperature-dependent luminescence spectra and decays. Finally, these clusters display TADF-based CPL signals at 575 nm (excited at 370 nm) with a g_{lum} of ~ 4×10^{-3}.

Phosphorescence CPL

As for the origin of photoluminescence, phosphorescence is an important complementary mechanism to fluorescence. Phosphorescence is the emission from triplet-excited states and its lifetime is longer than fluorescence. Therefore, phosphorescence is appealing in optical sensors, information security, optoelectronic devices and biomedical agents.

Phosphorescence can be observed in lanthanide and Cr ions at room temperature. As demonstrated in Figure 12B Hao *et al.*[81] reported a simple method to obtain colorful CPL-active inorganic persistent lanthanide-based phosphor materials with a long afterglow, including a yellow-green $SrAl_2O_4$:Eu,Dy, purple $CaAl_2O_4$:Eu,Nd, blue-green $Sr_4Al_4O_{25}$:Eu,Dy, sky blue $Sr_2MgSi_2O_7$ and red Y_2O_2S:Eu,Mg,Ti. These commercial phosphor powders are mixed with D- (or L-) cysteine (Cys) in ethanol and subjected to ball-milling for several hours and then the D-/L-Cys-modified phosphors are collected. Using this simple process, these phosphors became CPL-active with a $|g_{lum}|$ of 10^{-3}-10^{-2}, of which a maximum value was observed in the $CaAl_2O_4$:Eu,Nd sample (2.10×10^{-2}). The CD and CPL activity of these inorganic phosphors was induced by chiral Cys molecules, which were absorbed *via* metal-sulfur bonds.

Compared with lanthanides ions, the observation of room-temperature phosphorescence on other luminescent materials is not straightforward. Xu *et al.*[52] demonstrated a three-component system with both fluorescence- and phosphorescence-based CPL of carbon dots (CDs) at room temperature [Figure 12C]. Cellulose nanocrystals are used to form chiral photonic films, in which poly(vinyl alcohol) (PVA) and luminescent CDs are integrated by a co-assembly process. Because of the PBG effect, CPL was observed when the fluorescence wavelength (460 nm, excited by 365 nm) of the CDs located within the bandgap. The employment of PVA seemed to restrict molecular motions and inhibit oxygen quenching to maintain triplet excitons, thus leading to phosphorescence afterglow (480-500 nm) lasting for 2 s, even after turning off the UV (260 nm) irradiation. However, there is an overlap between the fluorescence spectrum (with a peak located at 450-470 nm) and the room-temperature phosphorescence (RTP) spectrum (with a peak at 480-500 nm). In other words, the fluorescence bands are close to the RTP bands. Therefore, it is difficult to differentiate FL-based CPL from RTP-induced CPL on the as-used JASCO CPL-200 spectrophotometer. These authors designed an analytical device [shown in Figure 12C, middle] to measure circular polarized room-temperature phosphorescence (CPRTP), which is fulfilled by combining a fluorospectrophotometer and an L- (or R-) circularly polarized filter (CPF). The CPF was covered on the detector at the

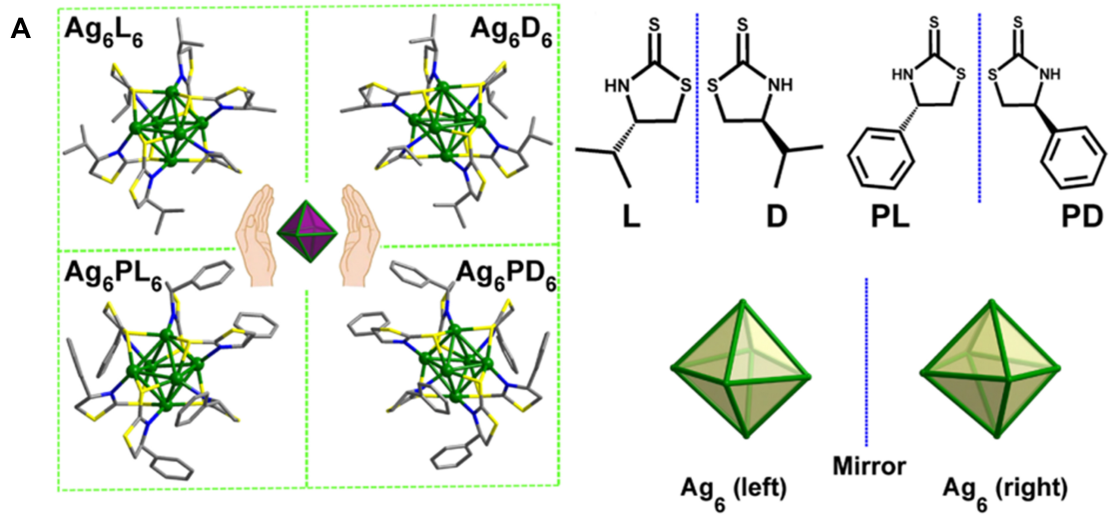
A
Ag_6L_6
Ag_6D_6
Ag_6PL_6
Ag_6PD_6
L
D
PL
PD
Ag_6 (left)
Mirror
Ag_6 (right)

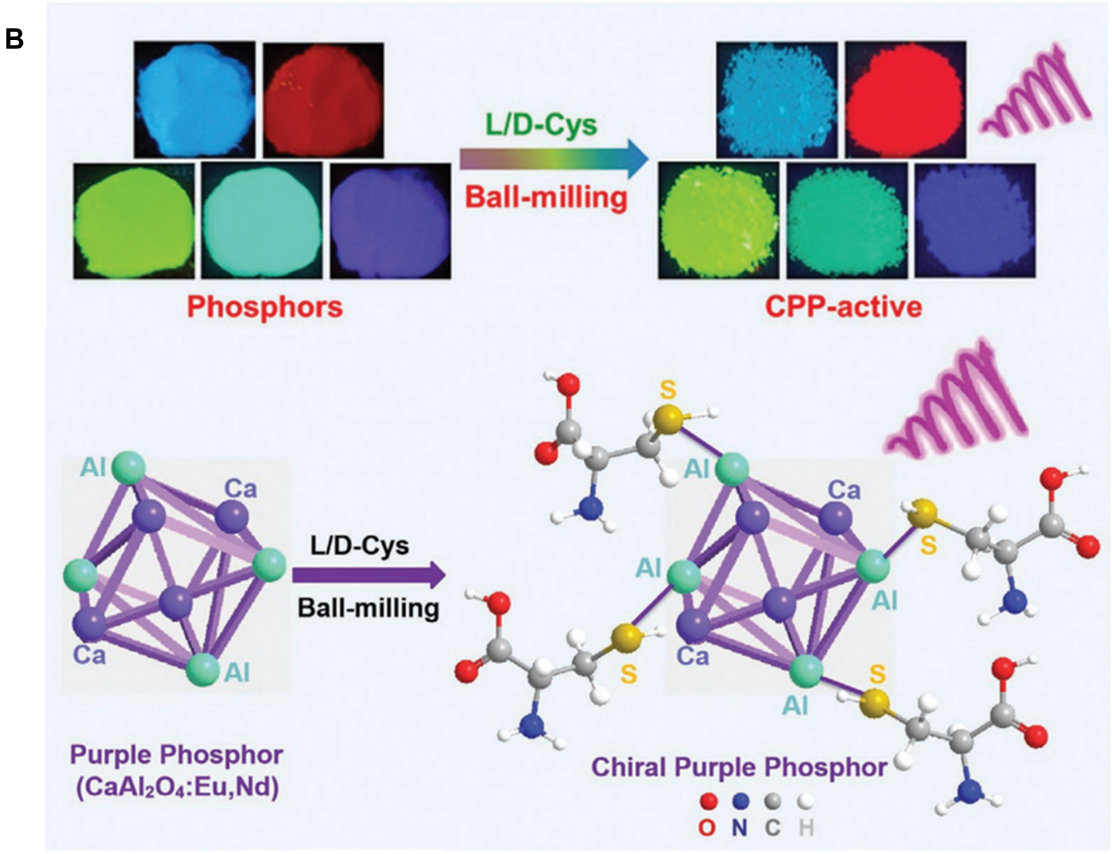
B
L/D-Cys
Ball-milling
Phosphors
CPP-active
Al
Ca
L/D-Cys
Ball-milling
Purple Phosphor
($CaAl_2O_4$:Eu,Nd)
Chiral Purple Phosphor
O N C H

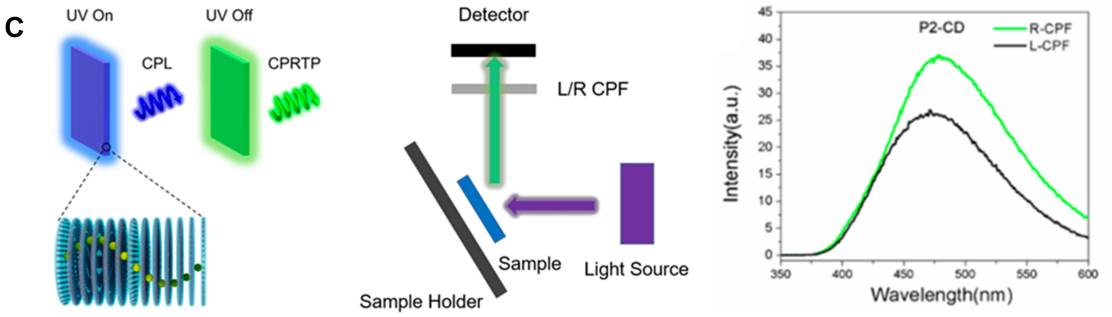
C
UV On
UV Off
CPL
CPRTP
Detector
L/R CPF
Sample
Light Source
Sample Holder
P2-CD
R-CPF
L-CPF
Intensity(a.u.)
Wavelength(nm)

Figure 12. (A) Structures of Ag_6L_6/D_6 and Ag_6PL_6/PD_6 enantiomers, L/D, PL/PD and octahedral Ag_6 framework in Ag_6L_6/D_6. Reproduced with permission from Ref.[80]. (B) Images of various lanthanide-containing phosphor materials before and after modification with L/D-Cys via ball milling (top) and schematic of $CaAl_2O_4$:Eu,Nd phosphor attached by chiral Cys molecules on the surface and the induction of the phosphorescence-based CPL (bottom). Reproduced with permission from Ref.[81]. Copyright (2021) John Wiley and Sons. (C) Schematic of hybrid chiral photonic showing dual CPL and CPRTP (left), an experimental setup for the measurement of CPRTP (middle) and phosphorescence emission spectra of hybrid chiral photonic films recorded with an L-CPF or R-CPF (right). Reproduced with permission from Ref.[52]. Copyright (2020) American Chemical Society. CPL: Circularly polarized luminescence; CPRTP: circular polarized room-temperature phosphorescence; CPF: circularly polarized filter.

phosphorescence measurement mode to record the CPRTP spectra. In principle, L-CPRTP would be blocked by the RCPF, while R-CPRTP would be blocked by the LCPF. On this basis, it was found that the CPRTP intensity recorded with LCPF was weaker than RCPF. By borrowing the definition of g_{lum}, a so-called g_{RTP} is defined as $g_{RTP} = [2\times(I_L-I_R)]/(I_L+I_R)$, where I_L and I_R are the intensity of RTP recorded under LCPF and RCPF, respectively. The highest absolute value of g_{RTP} could reach 0.461.

APPLICATIONS OF INORGANIC-ASSOCIATED CPL

With success in the synthesis of various inorganic-associated CPL-active systems, their potential applications are also explored. Here, we list several examples related to sensors, security, electroluminescent devices, optical storage and asymmetric synthesis.

Sensors

Fluorescence sensing is an important analysis technique with many merits, such as rapidness, sensitivity, nondestructiveness and the ability to obtain diverse information regarding molecular interactions and microenvironments. Since fluorescence is a prerequisite for CPL, the change in fluorescent properties leads to the variation of CPL signals. Therefore, the principles of fluorescence sensing may be borrowed to design CPL sensors. For example, Suo *et al.*[82] reported a AuAg bimetallic cluster-based CPL sensing method by virtue of the fluorescence quenching effect [Figure 13A]. In the presence of metal ions (Sr^{2+} and K^+), guanosine 5′-monophosphate can self-assemble into left- or right-handed helical nanofibers (g-fibers) with a width of 200 nm and a length of several micrometers. These g-fibers are used as chiral hosts to embed AuAg clusters stabilized with adenosine 5′-monophosphate. Consequently, helical nanostructured g-fiber-AuAg composites were obtained and showed CPL at ~ 475 nm under a 356 nm excitation, with a $|g_{lum}|$ of 1-3×10^{-2}. Because of the fluorescence quenching of AuAg NCs by L-Cys, g-fiber-AuAg NCs could be used as CPL sensors for the selective detection of L-Cys (in the range of 0.1 to 8 μmol L^{-1}) with a limit of detection down to 95.7 nM, which is comparable to other common fluorometric and electrochemical methods.

Anticounterfeiting

Luminescent nanomaterials are widely employed in anticounterfeiting applications. To improve the security level, it is highly desirable that a luminescent material can possess more features. CPL-active materials encode hidden chiral fingerprint information into luminescence, which is not easily decoded by common optical read-out instruments. As a result, CPL offers a novel advanced anticounterfeiting technique with high expertise in chirality.

Kitagawa *et al.*[83] firstly synthesized europium complexes with chiral (+/-)-3-(trifluoroacetyl)camphor (+/-tfc) ligands and then cast them on a glass substrate together with the achiral glass promoter tris(2,6-dimethoxyphenyl)phosphine oxide (tmpo) ligand [Figure 13B]. After solvent evaporation, two enantiomeric Eu(+tfc)-tmpo(2) and Eu (–tfc)-tmpo(2) transparent films with an extra-large $|g_{lum}|$ of 1.2 at a 594 nm emission (the magnetic dipole transition $^5D_0 \rightarrow {}^7F_1$ of Eu^{3+}) were produced. Furthermore, the authors demonstrated a CP light-based security device model to visualize the CPL image by a camera equipped with a linear polarizer, a rotatable λ/4 plate and a bandpass filter (594 nm). Eu(+tfc)-tmpo(2) was cast into a sun

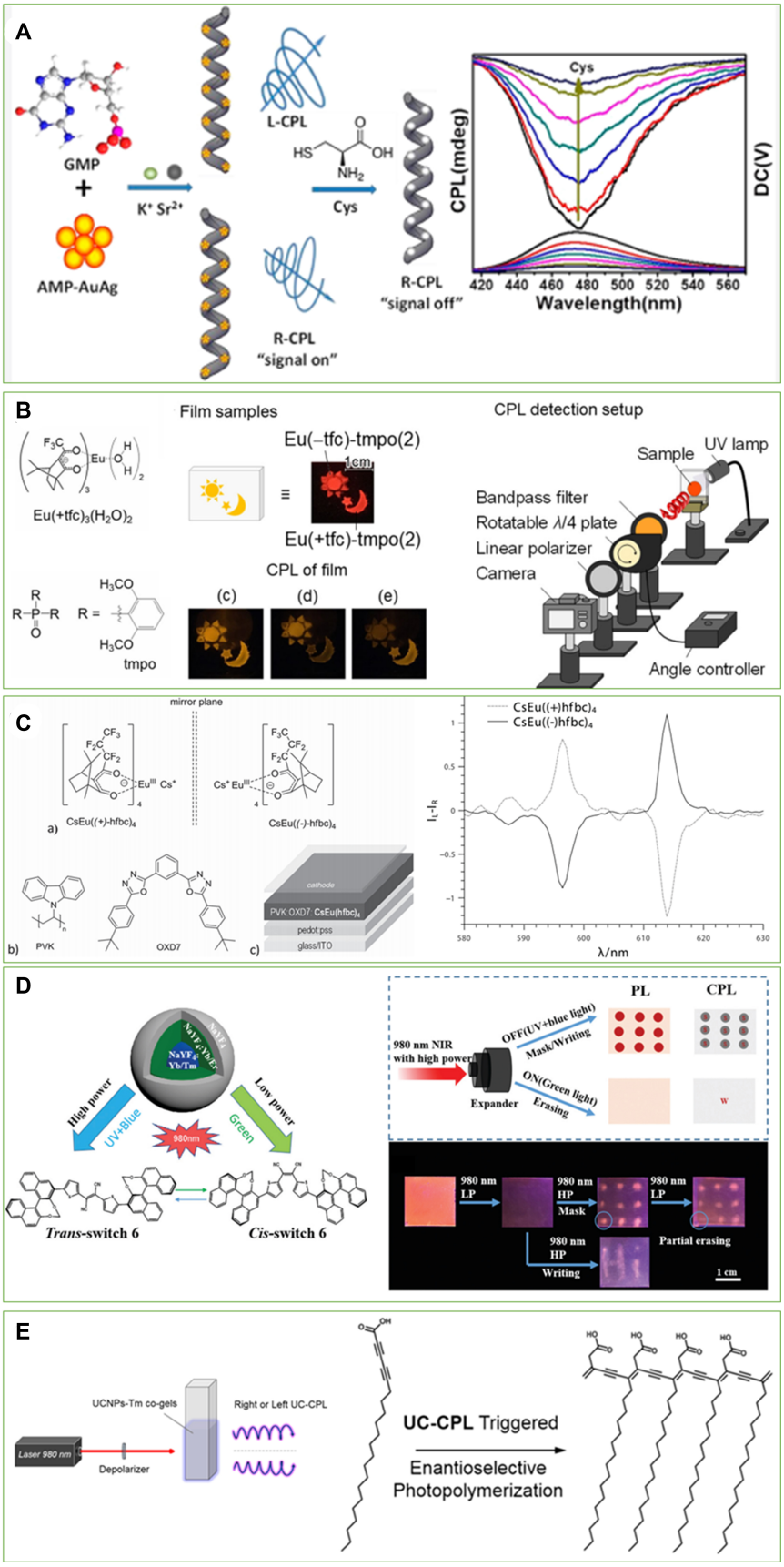
A
GMP
AMP-AuAg
K⁺ Sr²⁺
L-CPL
Cys
R-CPL
"signal off"
R-CPL
"signal on"
CPL(mdeg)
DC(V)
Wavelength(nm)
B
Film samples
Eu(+tfc)₃(H₂O)₂
Eu(−tfc)-tmpo(2)
Eu(+tfc)-tmpo(2)
tmpo
CPL of film
CPL detection setup
Sample
UV lamp
Bandpass filter
Rotatable λ/4 plate
Linear polarizer
Camera
Angle controller
C
mirror plane
CsEu((+)-hfbc)₄
CsEu((-)-hfbc)₄
PVK
OXD7
cathode
pedot:pss
glass/ITO
λ/nm
D
High power
UV+Blue
Low power
Green
980nm
Trans-switch 6
Cis-switch 6
PL
CPL
980 nm NIR with high power
Expander
OFF(UV+blue light)
Mask/Writing
ON(Green light)
Erasing
980 nm LP
980 nm HP
Mask
Writing
Partial erasing
1 cm
E
UCNPs-Tm co-gels
Right or Left UC-CPL
Laser 980 nm
Depolarizer
UC-CPL Triggered
Enantioselective
Photopolymerization

Figure 13. Applications of inorganic-associated CPL-active systems. (A) CPL sensors of Cys. Reproduced with permission from Ref.[82]. Copyright (2020) American Chemical Society. (B) A security paint based on CPL-active Eu(III) lumino-glass. Reproduced with permission from Ref.[83]. (C) Electroluminescent device architecture containing chiral Eu(III) complexes and their circularly polarized electroluminescence (CPEL) spectra. Reproduced with permission from Ref.[84]. Copyright (2015) John Wiley and Sons. (D) Conceptual description of illuminating PL/CPL dual-mode rewritable optical storage and real images of PL/CPL dual-mode patterns. Reproduced with permission from Ref. [87]. Copyright (2020) Royal Society of Chemistry. (E) Schematic of enantioselective photopolymerization setup of HA. Reproduced with permission from Ref.[88]. Copyright (2019) American Chemical Society. PL: Photoluminescence; CPL: circularly polarized luminescenc.

pattern and Eu(–tfc)-tmpo(2) into a moon. Without the λ/4 plate, both the sun and moon are observed. By rotating the λ/4 plate 90° clockwise or anticlockwise using an angle controller, the photographs of the emission using L-CP light ("sun") and R-CP light ("moon"), respectively, are exhibited.

Electroluminescent devices

Electroluminescent devices, where an emissive layer is sandwiched between an anode and a cathode, are promising for artificial light sources. In these devices, the charge carriers (electrons and holes) are generated at the electrodes under an external voltage, transported to and then recombined at the emissive layer to produce electroluminescence. Various luminescent materials are used as the emissive layers to construct electroluminescent devices, such as organic, CD-based and perovskite-based light emitting diodes. Furthermore, these devices, which are capable of directly emitting CP light, are of significant interest for their promising potential in displays with high-resolution, 3D imaging ability, improved brightness and lower energy consumption.

Zinna *et al.*[84] used chiral europium complexes of $CsEu(hfbc)_4$ (hfbc = 3-heptafluoro-butylyrylcamphorate) with the highest available g_{lum} (g_{lum} = 1.38 at 595 nm) as circularly polarized emitters in electroluminescent devices [Figure 13C]. To reduce the emission from the matrix, the Eu(III) complexes were blended with a polyvinylcarbazole host and a soluble additive of 1,3-bis[2-(4-tert-butylphenyl)-1,3,4-oxadiazo-5-yl]benzene to form the emitting layer. To minimize the internal reflection of the emitted light on the back electrode, a Ba/Al cathode (50% transmittance at 612 nm) was employed. With these strategies, a good polarization degree of emission (as measured by the dissymmetry factor of g_{EL} in electroluminescence) is achieved, with g_{EL} values of ±0.75 and –0.09/+0.15 for the Eu $^5D_0 \rightarrow {}^7F_1$ (at 595 nm) and Eu $^5D_0 \rightarrow {}^7F_2$ transitions (at 612 nm), respectively. Furthermore, by optimizing the emissive layer formulations and fine-tuning the architectures of the devices, the absolute value of g_{EL} could even be increased to 1.0 (for Eu $^5D_0 \rightarrow {}^7F_1$ at 595 nm)[85].

Han *et al.*[86] reported two enantiomeric gold clusters $(Au_4L_4)_n/(Au_4D_4)_n$ consisting of a Au_4 core and a chiral ligand, (S)-/(R)-4-isopropylthiazolidine-2-thione [abbreviated as L and D, structures shown in Figure 12A]. Through an aggregation- and crystallization-induced emission process, these aggregated gold nanoclusters showed a strong green emission centered at 507 nm with a photoluminescence quantum yield of 41.4% and intense CPL signals with $|g_{lum}|$ of 7.0×10^{-3}. These nanoclusters were employed as the chiral emissive layer to fabricate electroluminescent devices. The as-obtained device exhibited obvious green CPEL signals (driven at a voltage of 10 V) with a maximum external quantum efficiency of 1.5% and a dissymmetry factor ($|g_{EL}|$) of $4\text{-}7\times10^{-3}$.

Optical storage

The usage of CP light for optical storage is attractive due to the orthogonal characteristics of the polarization and uncomplicated optical system structures. Juan *et al.*[87] proposed an optical storage model based on 980 nm NIR-light triggered reversible CPL switching. A cholesteric liquid crystal with a self-organized helical superstructure was used as the host to load lanthanide (Yb^{3+}, Er^{3+} or Tm^{3+})-doped $NaYF_4$-based UCNPs and a chiral fluorescent photoswitch of **6** [Figure 13D]. When the UCNPs are irradiated by 980 nm at a low

power (980-l), the 520 nm green emission ($Yb^{3+} \rightarrow Er^{3+}$ energy transfer process) dominated, while the 365 and 450 nm emissions ($Yb^{3+} \rightarrow Tm^{3+}$ energy transfer process) appeared at a high laser power density (980 h). Switch **6** showed a *trans* to *cis* photoisomerization under 520 nm light and the reverse isomerization upon irradiation at 365 or 450 nm. A strong emission peak at ~ 580 nm appeared for the *trans* state of switch **6** and greatly decreased for the *cis* state. Correspondingly, both the CPL signal and its absolute g_{lum} of ~ 580 nm decreased with low-power 980 nm NIR light, while partly recovering when exposed to high-power 980 nm light. Based on this switchable process controlled by laser power, a PL/CPL-encryption dual-mode rewritable optical storage device can be designed. The fluorescent dot array can be written on the cell using a photomask with a high-power laser and the information is erased under a low-power mode.

Asymmetric synthesis

CP light-induced asymmetric photochemical synthesis is an important type of absolute synthesis and even accounts for the homochirality origin on earth. Because of the unbalance between L- and R-CP emissions, CPL-active emitters are potential CP light sources to initiate enantioselective synthesis. Jin *et al.*[88] showed an up-conversion CPL to trigger the enantioselective polymerization of diacetylene [Figure 13E]. Achiral lanthanide-doped UCNPs ($NaYF_4$:Yb/Er or $NaYF_4$:Yb/Tm) were co-assembled with chiral lipid gelator L-/D-GAm to create helical nanotubes. After excitation with a 980 nm laser, the emission peaks of UCNPs-Tm are mainly located at 360 nm ($^1D_2 \rightarrow {}^3H_6$ transition), 476 nm ($^1G_4 \rightarrow {}^3H_6$) and 802 nm ($^3H_4 \rightarrow {}^3H_6$). Interestingly, the UV part of CPL from UCNPs-Tm could induce the polymerization of 2,4-heneicosadiynoic acid into polydiacetylene (PDA). PDA formed using L-GAm/UCNPs-Tm showed positive CD signals, while negative CD signals were found with D-GAm/UCNPs-Tm. Therefore, the molecular chirality of the gelator controlled the handedness of the UC-CPL from lanthanide ions and then subsequently regulated the enantioselective polymerization of diacetylene.

SUMMARY AND OUTLOOK

After a survey of the recent literature, it is without doubt that we have a toolbox to engineer multiple inorganic species (lanthanide ions, metal clusters, semiconductor NPs, carbon dots, perovskite NCs, nano-silica and so on) to undergo CPL, although they are not supposed to be chiral from our common sense. CPL in these inorganic materials is also found in various luminescence processes (e.g., up-conversion, TADF, phosphorescence and NIR emission) and is useful for many applications in sensing, optical storage, security and asymmetric synthesis. Because CPL is related to both chirality and luminescence, the achievements above prompt us to believe that two enantiomeric forms are allowed both in the structures and luminescence of inorganic substances and will open up new chirality-related horizons in inorganic chemistry and light science.

However, there are still many issues to be addressed to comprehend CPL in inorganics, including:

Reliable CPL data free from artifacts: CPL measurements are traditionally conducted on various homemade instruments and have recently been performed on some commercial CPL spectrophotometers. However, there are some artifacts possibly existing in as-measured CPL signals, which can be caused by many factors (e.g., instrumental limitations, linear dichroism effect and scattering/absorption phenomena). In particular, solid-state or anisotropic samples should be treated carefully. To this end, some experimental guides and data analysis methods can be found to obtain true CPL signals[89-93]. In addition, it is encouraging to give CD/PL spectra and some experimental details (e.g., sample concentrations and spectral test parameters) together with CPL data. It will be helpful to check the reliability and reproducibility of CPL signals.

Enhancement of g_{lum}: As shown in Table 1, the g_{lum} values of many kinds of inorganic-associated CPL are ~ 10^{-3} or lower, although some metal ions (e.g., lanthanide and chromium(III)) can potentially present high g_{lum} due to magnetically allowed but electric-dipole forbidden emissions. The small g_{lum} value means that the differences between LCP and RCP only account for 0.3% of the total emission. Hence, there is a significant potential to increase g_{lum}. Some enhancement strategies have been proposed, which are fulfilled by ingenious molecular design, energy transfer processes, plasmonic metal-assisted enhancement and assembly-/aggregation-induced CPL[19,94-97].

Evaluation indexes for CPL: Basically, CPL is based on luminescence and therefore the indexes for luminescence, such as quantum yield, brightness, excitation and emission wavelengths, should be taken into consideration together with g_{lum}. For example, Eu complexes showed a highest g_{lum} of 1.38 but with a very low emission quantum yield of less than 1.0%, which restricts their applications, especially in displays. The choice of excitation wavelength is also important in improving the CPL performance in some luminescent systems involved with energy transfer (e.g., metal complexes). Moreover, the relationships between g_{lum} and the luminescence parameters above are underexplored. Some researchers have suggested several indexes, such as a figure of merit (FM) (FM = $\Phi \times g_{lum}$, where Φ is the emission efficiency), asymmetric quantum efficiency (φ_a) ($\varphi_a = I_L/I_0$ or I_R/I_0, where I_0 is the incident light intensity) and a brightness indicator (BF) ($B_{CPL} = \varepsilon_\lambda \times \Phi \times g_{lum}/2$, where ε_λ is the molar coefficient measured at the excitation wavelength)[21,98,99]. Nevertheless, the application of the indexes above is underexplored for different purposes.

Multiple-component CPL-active systems: In many cases, the system is constructed as a binary-component mode, i.e., only one chiral entity and only a luminescent one. However, it is not easy to achieve an ideal CPL effect (e.g., high g_{lum}, strong emission and tunable emission bands) only by two components. Consequently, multiple components can be introduced to manipulate the optical and chiral properties.

Revealing the detailed mechanisms for CPL: Although we know how to synthesize CPL-active materials, the underlying mechanism is not well explained in many publications. Often, the chirality transfer/induction mechanisms proposed for CD activity are roughly extended to CPL activity, but it is unsuitable in some cases because CD and CPL belong to two different transition processes. In addition, the theories and simulation methods addressing luminescence in a chiral environment are currently inadequate.

Exploration of CPL-based applications: The applications described here are still in their infancy but are inspirational nonetheless. With success in materials synthesis, exploration of their real applications is an important follow-up work.

DECLARATIONS

Authors' contributions

Prepared and corrected the manuscript: Liu X, Jin RH

Availability of data and materials

Not applicable.

Financial support and sponsorship

The research was supported in part by the JSPS KAKENHI, grant number: JP16H06515 (Coordination Asymmetry) and by the JSPS KAKEHI Grantin-Aid for Scientific Research (B), 19H02767.

Conflicts of interest

Both authors declared that there are no conflicts of interest.

Ethical approval and consent to participate

Not applicable.

Consent for publication

Not applicable.

Copyright

REFERENCES

1. Guijarro A, Yus M. The origin of chirality in the molecules of life: a revision from awareness to the current theories and perspectives of this unsolved problem. Cambridge: Royal Society of Chemistry; 2009. DOI
2. Carreira EM, Yamamoto H. Comprehensive chirality. Elsevier: London; 2012. Available from: https://www.elsevier.com/books/comprehensive-chirality/yamamoto/978-0-08-095167-6. [Last accessed on 17 Mar 2022].
3. Stanciu CD, Hansteen F, Kimel AV, et al. All-optical magnetic recording with circularly polarized light. *Phys Rev Lett* 2007;99:047601. DOI PubMed
4. Kim S, Kim E. Performance analysis of stereoscopic three-dimensional projection display systems. *3D Res* 2010;1:1-16. DOI
5. Kunnen B, Macdonald C, Doronin A, Jacques S, Eccles M, Meglinski I. Application of circularly polarized light for non-invasive diagnosis of cancerous tissues and turbid tissue-like scattering media. *J Biophotonics* 2015;8:317-23. DOI PubMed
6. Krupová M, Kapitán J, Bouř P. Induced lanthanide circularly polarized luminescence as a probe of protein fibrils. *ACS Omega* 2019;4:1265-71. DOI PubMed PMC
7. Yang G, Zhang S, Hu J, Fujiki M, Zou G. The chirality induction and modulation of polymers by circularly polarized light. *Symmetry* 2019;11:474. DOI
8. Qu A, Sun M, Kim JY, et al. Stimulation of neural stem cell differentiation by circularly polarized light transduced by chiral nanoassemblies. *Nat Biomed Eng* 2021;5:103-13. DOI PubMed
9. Nishizawa N, Munekata H. Lateral-type spin-photonics devices: development and applications. *Micromachines (Basel)* 2021;12:644. DOI PubMed PMC
10. Zhan X, Xu FF, Zhou Z, Yan Y, Yao J, Zhao YS. 3D laser displays based on circularly polarized lasing from cholesteric liquid crystal arrays. *Adv Mater* 2021;33:e2104418. DOI PubMed
11. Jiang S, Xiong X, Hu Y, et al. High-efficiency generation of circularly polarized light via symmetry-induced anomalous reflection. *Phys Rev B* 2015:91. DOI
12. Zinna F, Pescitelli G, Di Bari L. Circularly polarized light at the mirror: caveats and opportunities. *Chirality* 2020;32:765-9. DOI PubMed
13. Ranjbar B, Gill P. Circular dichroism techniques: biomolecular and nanostructural analyses- a review. *Chem Biol Drug Des* 2009;74:101-20. DOI PubMed
14. MacKenzie LE, Pålsson LO, Parker D, Beeby A, Pal R. Rapid time-resolved circular polarization luminescence (CPL) emission spectroscopy. *Nat Commun* 2020;11:1676. DOI PubMed PMC
15. Riehl JP, Muller G. Circularly Polarized Luminescence Spectroscopy and Emission-Detected Circular Dichroism. In: Berova N, Polavarapu PL, Nakanishi K, Woody RW, editors. Comprehensive Chiroptical Spectroscopy. John Wiley & Sons, Inc.; 2011. p.65-90. DOI
16. Sánchez-Carnerero EM, Agarrabeitia AR, Moreno F, et al. circularly polarized luminescence from simple organic molecules. *Chemistry* 2015;21:13488-500. DOI PubMed PMC
17. Ma JL, Peng Q, Zhao CH. Circularly polarized luminescence switching in small organic molecules. *Chemistry* 2019;25:15441-54. DOI PubMed
18. Nitti A, Pasini D. Aggregation-induced circularly polarized luminescence: chiral organic materials for emerging optical technologies. *Adv Mater* 2020;32:e1908021. DOI PubMed
19. Sang Y, Han J, Zhao T, Duan P, Liu M. Circularly polarized luminescence in nanoassemblies: generation, amplification, and application. *Adv Mater* 2020;32:e1900110. DOI PubMed
20. Zhang DW, Li M, Chen CF. Recent advances in circularly polarized electroluminescence based on organic light-emitting diodes. *Chem Soc Rev* 2020;49:1331-43. DOI PubMed
21. Deng Y, Wang M, Zhuang Y, Liu S, Huang W, Zhao Q. Circularly polarized luminescence from organic micro-/nano-structures. *Light Sci Appl* 2021;10:76. DOI PubMed PMC
22. Gong Z, Zhu X, Zhou Z, et al. Frontiers in circularly polarized luminescence: molecular design, self-assembly, nanomaterials, and

applications. *Sci China Chem* 2021;64:2060-104. DOI
23. Jiang S, Kotov NA. Circular polarized light emission in chiral inorganic nanomaterials. *Adv Mater* 2022:e2108431. DOI PubMed
24. Sun M, Xu L, Qu A, et al. Site-selective photoinduced cleavage and profiling of DNA by chiral semiconductor nanoparticles. *Nat Chem* 2018;10:821-30. DOI PubMed
25. Vinegrad E, Hananel U, Markovich G, Cheshnovsky O. Determination of handedness in a single chiral nanocrystal via circularly polarized luminescence. *ACS Nano* 2019;13:601-8. DOI PubMed
26. Hananel U, Ben-Moshe A, Diamant H, Markovich G. Spontaneous and directed symmetry breaking in the formation of chiral nanocrystals. *Proc Natl Acad Sci U S A* 2019;116:11159-64. DOI PubMed PMC
27. Hao J, Li Y, Miao J, et al. Ligand-induced chirality in asymmetric CdSe/CdS nanostructures: a close look at chiral tadpoles. *ACS Nano* 2020;14:10346-58. DOI PubMed
28. Krishnadas KR, Sementa L, Medves M, et al. Chiral functionalization of an atomically precise noble metal cluster: insights into the origin of chirality and photoluminescence. *ACS Nano* 2020;14:9687-700. DOI PubMed
29. Ben-Moshe A, Govorov AO, Markovich G. Enantioselective synthesis of intrinsically chiral mercury sulfide nanocrystals. *Angew Chem Int Ed Engl* 2013;52:1275-9. DOI PubMed
30. Morrow SM, Bissette AJ, Fletcher SP. Transmission of chirality through space and across length scales. *Nat Nanotechnol* 2017;12:410-9. DOI PubMed
31. Kim H, Im SW, Kim RM, et al. Chirality control of inorganic materials and metals by peptides or amino acids. *Mater Adv* 2020;1:512-24. DOI
32. Dryzun C, Mastai Y, Shvalb A, Avnir D. Chiral silicate zeolites. *J Mater Chem* 2009;19:2062. DOI
33. Riehl JP, Richardson FS. Circularly polarized luminescence spectroscopy. *Chem Rev* 1986;86:1-16. DOI
34. Moran DM, Metcalf DH, Richardson FS. Chiroptical luminescence spectra of uranyl ion in cubic sodium tris(acetato)dioxouranate(1-) crystals. *Inorg Chem* 1992;31:819-25. DOI
35. Mukhina MV, Maslov VG, Baranov AV, et al. Intrinsic chirality of CdSe/ZnS quantum dots and quantum rods. *Nano Lett* 2015;15:2844-51. DOI PubMed
36. Duan Y, Han L, Zhang J, et al. Optically active nanostructured ZnO films. *Angew Chem Int Ed Engl* 2015;54:15170-5. DOI PubMed
37. Flack H. Chiral and achiral crystal structures. *HCA* ;86:905-21. DOI PubMed
38. Gautier R, Klingsporn JM, Van Duyne RP, Poeppelmeier KR. Optical activity from racemates. *Nat Mater* 2016;15:591-2. DOI PubMed
39. Zhao J, Zhang T, Dong XY, et al. Circularly polarized luminescence from achiral single crystals of hybrid manganese halides. *J Am Chem Soc* 2019;141:15755-60. DOI PubMed
40. Kumar J, Thomas KG, Liz-Marzán LM. Nanoscale chirality in metal and semiconductor nanoparticles. *Chem Commun (Camb)* 2016;52:12555-69. DOI PubMed PMC
41. Tohgha U, Deol KK, Porter AG, et al. Ligand induced circular dichroism and circularly polarized luminescence in CdSe quantum dots. *ACS Nano* 2013;7:11094-102. DOI PubMed PMC
42. Maoz BM, Chaikin Y, Tesler AB, et al. Amplification of chiroptical activity of chiral biomolecules by surface plasmons. *Nano Lett* 2013;13:1203-9. DOI PubMed
43. Ben-Moshe A, Maoz BM, Govorov AO, Markovich G. Chirality and chiroptical effects in inorganic nanocrystal systems with plasmon and exciton resonances. *Chem Soc Rev* 2013;42:7028-41. DOI PubMed
44. Cao Z, Gao H, Qiu M, et al. Chirality transfer from sub-nanometer biochemical molecules to sub-micrometer plasmonic metastructures: physiochemical mechanisms, biosensing, and bioimaging opportunities. *Adv Mater* 2020;32:e1907151. DOI PubMed
45. Lunkley JL, Shirotani D, Yamanari K, Kaizaki S, Muller G. Extraordinary circularly polarized luminescence activity exhibited by cesium tetrakis(3-heptafluoro-butylryl-(+)-camphorato) Eu(III) complexes in EtOH and CHCl3 solutions. *J Am Chem Soc* 2008;130:13814-5. DOI
46. Wong H, Lo W, Yim K, Law G. Chirality and chiroptics of lanthanide molecular and supramolecular assemblies. *Chem* 2019;5:3058-95. DOI
47. Staszak K, Wieszczycka K, Marturano V, Tylkowski B. Lanthanides complexes – Chiral sensing of biomolecules. *Coordination Chemistry Reviews* 2019;397:76-90. DOI
48. Mackenzie LE, Pal R. Circularly polarized lanthanide luminescence for advanced security inks. *Nat Rev Chem* 2021;5:109-24. DOI
49. Jiménez JR, Poncet M, Míguez-Lago S, et al. Bright long-lived circularly polarized luminescence in chiral chromium(III) complexes. *Angew Chem Int Ed Engl* 2021;60:10095-102. DOI PubMed
50. Poncet M, Benchohra A, Jiménez J, Piguet C. Chiral chromium(III) complexes as promising candidates for circularly polarized luminescence. *ChemPhotoChem* 2021;5:880-92. DOI
51. Ru Y, Ai L, Jia T, et al. Recent advances in chiral carbonized polymer dots: From synthesis and properties to applications. *Nano Today* 2020;34:100953. DOI
52. Xu M, Wu X, Yang Y, et al. Designing hybrid chiral photonic films with circularly polarized room-temperature phosphorescence. *ACS Nano* 2020;14:11130-9. DOI PubMed
53. Chekini M, Prince E, Zhao L, Mundoor H, Smalyukh II, Kumacheva E. Chiral carbon dots synthesized on cellulose nanocrystals. *Adv Optical Mater* 2020;8:1901911. DOI
54. Li A, Zheng D, Zhang M, Wu B, Zhu L. Chirality transfer in carbon dot-composited Sol-gel systems for excitation-dependent

circularly polarized luminescence. *Langmuir* 2020;36:8965-70. DOI PubMed

55. Ru Y, Sui L, Song H, et al. Rational design of multicolor-emitting chiral carbonized polymer dots for full-color and white circularly polarized luminescence. *Angew Chem Int Ed Engl* 2021;60:14091-9. DOI PubMed
56. Zhang M, Li K, Zang S. Progress in atomically precise coinage metal clusters with aggregation-induced emission and circularly polarized luminescence. *Adv Optical Mater* 2020;8:1902152. DOI
57. Wu H, He X, Yang B, Li CC, Zhao L. Assembly-induced strong circularly polarized luminescence of spirocyclic chiral silver(I) clusters. *Angew Chem Int Ed Engl* 2021;60:1535-9. DOI PubMed
58. Zhang MM, Dong XY, Wang ZY, et al. AIe triggers the circularly polarized luminescence of atomically precise enantiomeric copper(I) Alkynyl Clusters. *Angew Chem Int Ed Engl* 2020;59:10052-8. DOI PubMed
59. Shi L, Zhu L, Guo J, et al. Self-assembly of chiral gold clusters into crystalline nanocubes of exceptional optical activity. *Angew Chem Int Ed Engl* 2017;56:15397-401. DOI PubMed
60. Tao J, Li B, Lu Z, et al. Endowing zeolite lta superballs with the ability to manipulate light in multiple ways. *Angew Chem Int Ed Engl* 2020;59:19684-90. DOI PubMed
61. Bobrovsky A, Mochalov K, Oleinikov V, et al. Optically and electrically controlled circularly polarized emission from cholesteric liquid crystal materials doped with semiconductor quantum dots. *Adv Mater* 2012;24:6216-22. DOI PubMed
62. Yan J, Ota F, San Jose BA, Akagi K. Chiroptical resolution and thermal switching of chirality in conjugated polymer luminescence via selective reflection using a double-layered cell of chiral nematic liquid crystal. *Adv Funct Mater* 2017;27:1604529. DOI
63. Wang C, Chen K, Xu P, Yeung F, Kwok H, Li G. Fully chiral light emission from Cspbx $_3$ perovskite nanocrystals enabled by cholesteric superstructure stacks. *Adv Funct Mater* 2019;29:1903155. DOI
64. Cheng J, Hao J, Liu H, et al. Optically active CdSe-Dot/CdS-Rod nanocrystals with induced chirality and circularly polarized luminescence. *ACS Nano* 2018;12:5341-50. DOI PubMed
65. Dong Y, Zhang Y, Li X, Feng Y, Zhang H, Xu J. Chiral perovskites: promising materials toward next-generation optoelectronics. *Small* 2019;15:e1902237. DOI PubMed
66. Long G, Sabatini R, Saidaminov MI, et al. Chiral-perovskite optoelectronics. *Nat Rev Mater* 2020;5:423-39. DOI
67. Ma S, Ahn J, Moon J. Chiral perovskites for next-generation photonics: from chirality transfer to chiroptical activity. *Adv Mater* 2021;33:e2005760. DOI PubMed
68. Jin RH. Understanding silica from the viewpoint of asymmetry. *Chemistry* 2019;25:6270-83. DOI PubMed
69. Matsukizono H, Jin RH. High-temperature-resistant chiral silica generated on chiral crystalline templates at neutral pH and ambient conditions. *Angew Chem Int Ed Engl* 2012;51:5862-5. DOI PubMed
70. Harada T, Yanagita H, Ryu N, et al. Lanthanide ion-doped silica nanohelix: a helical inorganic network acts as a chiral source for metal ions. *Chem Commun (Camb)* 2021;57:4392-5. DOI PubMed
71. Sugimoto M, Liu XL, Tsunega S, et al. Circularly polarized luminescence from inorganic materials: encapsulating guest lanthanide oxides in chiral silica hosts. *Chemistry* 2018;24:6519-24. DOI PubMed
72. Tsunega S, Jin RH, Nakashima T, Kawai T. Transfer of chiral information from silica hosts to achiral luminescent guests: a simple approach to accessing circularly polarized luminescent systems. *Chempluschem* 2020;85:619-26. DOI PubMed
73. Liu P, Chen W, Okazaki Y, et al. Optically active perovskite Cspbbr$_3$ nanocrystals helically arranged on inorganic silica nanohelices. *Nano Lett* 2020;20:8453-60. DOI PubMed
74. Cai X, Du J, Zhang L, et al. Circularly polarized luminescence of single-handed helical tetraphenylethylene-silica nanotubes. *Chem Commun (Camb)* 2019;55:12176-9. DOI PubMed
75. Zhang W, Chang H, Ai J, Che S, Duan Y, Han L. Spontaneous chiral self-assembly of achiral AIEgens into AIEgen-silica hybrid nanotubes. *Chem Commun (Camb)* 2019;55:14438-41. DOI PubMed
76. Zhang S, Shi W, Rong S, Li S, Zhuang J, Wang X. Chirality evolution from Sub-1 nanometer nanowires to the macroscopic helical structure. *J Am Chem Soc* 2020;142:1375-81. DOI PubMed
77. Yang X, Zhou M, Wang Y, Duan P. Electric-field-regulated energy transfer in chiral liquid crystals for enhancing upconverted circularly polarized luminescence through steering the photonic bandgap. *Adv Mater* 2020;32:e2000820. DOI PubMed
78. Zinna F, Arrico L, Di Bari L. Near-infrared circularly polarized luminescence from chiral Yb(iii)-diketonates. *Chem Commun (Camb)* 2019;55:6607-9. DOI PubMed
79. Frédéric L, Desmarchelier A, Favereau L, Pieters G. Designs and applications of circularly polarized thermally activated delayed fluorescence molecules. *Adv Funct Mater* 2021;31:2010281. DOI
80. Han Z, Dong XY, Luo P, et al. Ultrastable atomically precise chiral silver clusters with more than 95% quantum efficiency. *Sci Adv* 2020;6:eaay0107. DOI PubMed PMC
81. Hao W, Li Y, Liu M. Endowing phosphor materials with long-afterglow circularly polarized phosphorescence via ball milling. *Adv Optical Mater* 2021;9:2100452. DOI
82. Suo Z, Hou X, Chen J, et al. Highly chiroptical detection with gold-silver bimetallic nanoclusters circularly polarized luminescence based on G-quartet nanofiber self-assembly. *J Phys Chem C* 2020;124:21094-102. DOI
83. Kitagawa Y, Wada S, Islam MDJ, et al. Chiral lanthanide lumino-glass for a circularly polarized light security device. *Commun Chem* 2020:3. DOI
84. Zinna F, Giovanella U, Di Bari L. Highly circularly polarized electroluminescence from a chiral europium complex. *Adv Mater* 2015;27:1791-5. DOI PubMed

85. Zinna F, Pasini M, Galeotti F, Botta C, Di Bari L, Giovanella U. Design of Lanthanide-based oleds with remarkable circularly polarized electroluminescence. *Adv Funct Mater* 2017;27:1603719. DOI
86. Han Z, Zhao X, Peng P, et al. Intercluster aurophilicity-driven aggregation lighting circularly polarized luminescence of chiral gold clusters. *Nano Res* 2020;13:3248-52. DOI
87. Juan A, Sun H, Qiao J, Guo J. Near-infrared light-controlled circularly polarized luminescence of self-organized emissive helical superstructures assisted by upconversion nanoparticles. *Chem Commun (Camb)* 2020;56:13649-52. DOI PubMed
88. Jin X, Sang Y, Shi Y, et al. Optically Active Upconverting nanoparticles with induced circularly polarized luminescence and enantioselectively triggered photopolymerization. *ACS Nano* 2019;13:2804-11. DOI PubMed
89. Longhi G, Castiglioni E, Koshoubu J, Mazzeo G, Abbate S. circularly polarized luminescence: a review of experimental and theoretical aspects. *Chirality* 2016;28:696-707. DOI PubMed
90. Chen W, Tian Z, Li Y, Jiang Y, Liu M, Duan P. Long-persistent circularly polarized phosphorescence from chiral organic ionic crystals. *Chemistry* 2018;24:17444-8. DOI PubMed
91. Tanaka H, Inoue Y, Mori T. Circularly polarized luminescence and circular dichroisms in small organic molecules: correlation between excitation and emission dissymmetry factors. *ChemPhotoChem* 2018;2:386-402. DOI
92. Castiglioni E, Abbate S, Lebon F, Longhi G. Ultraviolet, circular dichroism, fluorescence, and circularly polarized luminescence spectra of regioregular poly-[3-((S)-2-methylbutyl)-thiophene] in solution. *Chirality* 2012;24:725-30. DOI PubMed
93. Harada T, Kuroda R, Moriyama H. Solid-state circularly polarized luminescence measurements: theoretical analysis. *Chemical Physics Letters* 2012;530:126-31. DOI
94. Kumar J, Nakashima T, Tsumatori H, Kawai T. Circularly polarized luminescence in chiral aggregates: dependence of morphology on luminescence dissymmetry. *J Phys Chem Lett* 2014;5:316-21. DOI PubMed
95. Zhang C, Li S, Dong X, Zang S. Circularly polarized luminescence of agglomerate emitters. *Aggregate* 2021:2. DOI
96. Zhao S, Yu Y, Zhang B, et al. Metal-Enhanced circularly polarized luminescence of self-assembled Au@SiO_2 triangular nanoprisms and fluorophores in chiral cellulose nanocrystal films. *Adv Optical Mater* 2021;9:2100907. DOI
97. Greenfield JL, Wade J, Brandt JR, Shi X, Penfold TJ, Fuchter MJ. Pathways to increase the dissymmetry in the interaction of chiral light and chiral molecules. *Chem Sci* 2021;12:8589-602. DOI PubMed PMC
98. Yao L, Niu G, Li J, et al. Circularly polarized luminescence from chiral tetranuclear copper(I) iodide clusters. *J Phys Chem Lett* 2020;11:1255-60. DOI PubMed
99. Arrico L, Di Bari L, Zinna F. Quantifying the overall efficiency of circularly polarized emitters. *Chemistry* 2021;27:2920-34. DOI PubMed

Ren-Hua Jin

Ren-Hua Jin graduated from Jilin University (China) in 1982 and completed his PhD at Nankai University (China) in 1987. After that, he joined Beijing University of Chemical Technology as an assistant professor and then transferred to the University of Tokyo as a postdoctoral fellow. He worked at Miyazaki University as an associate professor (1994 ~ 1997). Then, he worked at the Kawamura Institute of Chemical Research as a leader for 14 years and moved to Kanagawa University as a full professor in April 2012. His current research interests lie in the architecture of water-soluble/amphiphilic polymers, the design of ceramic nanomaterials with shape- and/or chirality-control, and their applications in catalysis, separation, optical materials, sensing, etc.

Xinling Liu

Xinling Liu earned his bachelor's degree in chemistry from Ocean University of China in 2008. Then, he obtained his PhD degree in Physical Chemistry at Shanghai Institute of Ceramics, Chinese Academy of Sciences (SICCAS) in 2013. After postdoc research at Shanghai University and Kanagawa University, he joined the College of Chemistry and Materials Science at Shanghai Normal University in 2018 and became an associate professor. His current research interests lie in the synthesis of chiral inorganic nanomaterials and understanding their chiroptical properties (circular dichroism, circularly polarized luminescence), and the applications of Raman spectroscopy in chiral recognition.